

# POLITECNICO DI TORINO

Master's Degree in Mechanical Engineering



Master's Degree Thesis

## Thermal Modelling of a Fuel Cell System for an Electric Vehicle

Supervisors

Prof. Daniela Anna MISUL

Prof. Giovanni BELINGARDI

Dr. Pier Giuseppe ANSELMA

Eng. Matteo SPANO

Candidate

**Ilaria PRINCIPE**

December 2021



## **Abstract**

In the current global situation, organizations are required to achieve decarbonization. To reach this goal in the transportation field, one possible solution could be the electrification of vehicles. Fuel cells represent an optimal solution to pursue this goal.

This dissertation aims at developing a thermal model of a Proton Exchange Membrane Fuel Cell in a Simulink environment that will be later integrated into the hybrid powertrain of a heavy-duty vehicle. Thermal management is crucial for a fuel cell system, particularly in automotive applications. In fact, during load variations, temperature changes impact negatively the efficiency of the fuel cell to the extent that at high temperatures the functioning can be irreversibly compromised.

It has been implemented a lumped parameter approach for modeling the stack and the cooling system. The heat dissipated by the fuel cell allows to compute its temperature by solving the thermal circuit. To not overheat the fuel cell, a cooling system is integrated and it is composed mainly of pipes, a centrifugal pump and a radiator that releases a fraction of the heat into the surrounding environment.

The model is tested in dynamic conditions through a driving cycle and it is validated using the results obtained in a Siemens software, namely AMESim. The outcomes show similar trends in temperature between the two models with low error on the estimated thermal behaviour.



# Table of Contents

<b>List of Figures</b>	IV
<b>1 Introduction</b>	1
1.1 Hydrogen for heavy-duty transport . . . . .	1
1.2 Fuel Cells . . . . .	2
1.3 Aim of the work . . . . .	3
<b>2 Fuel Cells and Cooling System</b>	4
2.1 FC Working Principles . . . . .	4
2.2 FC Stack . . . . .	5
2.2.1 Bipolar Plates . . . . .	5
2.2.2 Gas Diffusion Layer . . . . .	6
2.2.3 Catalyst Layer . . . . .	7
2.2.4 Membrane . . . . .	8
2.3 Cell Voltage and efficiency . . . . .	9
2.4 Polarization curve . . . . .	10
2.4.1 Activation Losses . . . . .	11
2.4.2 Internal currents and crossover losses . . . . .	12
2.4.3 Ohmic losses . . . . .	13
2.4.4 Concentration losses . . . . .	13
2.4.5 Polarization curves . . . . .	15
2.5 Effects of Temperature . . . . .	16
2.6 Cooling system . . . . .	18
2.6.1 Stack heat balance . . . . .	19
2.6.2 Cooling systems . . . . .	20
<b>3 Simulink Model</b>	21
3.1 Stack . . . . .	22
3.1.1 Chemical voltage . . . . .	22
3.1.2 Cell Voltage . . . . .	24
3.1.3 Heat loss . . . . .	25

3.2	Cooling System . . . . .	26
3.2.1	Heat exchange . . . . .	26
3.2.2	Thermodynamic properties . . . . .	27
3.2.3	Heat exchange coefficient . . . . .	30
3.2.4	Centrifugal pump and pressure drops . . . . .	34
3.2.5	Radiator . . . . .	36
3.2.6	Cooling system control . . . . .	39
3.3	Model configuration . . . . .	41
<b>4</b>	<b>Results</b>	<b>43</b>
4.1	Heat generation . . . . .	44
4.2	Heat exchange . . . . .	47
4.3	Pump and pressure drops . . . . .	50
4.4	Radiator . . . . .	51
4.5	Temperature . . . . .	51
<b>5</b>	<b>Conclusions</b>	<b>54</b>
<b>A</b>	<b>Convective heat exchange coefficient</b>	<b>56</b>
	<b>Bibliography</b>	<b>58</b>

# List of Figures

2.1	FC reaction principles [5] . . . . .	5
2.2	Bipolar plates scheme [6] . . . . .	6
2.3	GDL carbon cloth on the left and carbon paper on the right [2] . .	7
2.4	Catalyst layer structure [3] . . . . .	7
2.5	FC Overall functioning [7] . . . . .	8
2.6	Structure of PFSA [2] . . . . .	9
2.7	Voltage loss due to polarization activation [2] . . . . .	11
2.8	Effect of internal currents and/or hydrogen crossover loss on open circuit potential [2] . . . . .	12
2.9	Resistive ohmic losses in the fuel cell [2] . . . . .	13
2.10	Concentration polarization losses in the fuel cell [2] . . . . .	14
2.11	Voltage losses in the fuel cell and the resulting polarization curve [2]	15
2.12	Effect of operating temperature on fuel cell polarization curve [2] . .	17
2.13	Different cooling options [2] . . . . .	18
2.14	Heat paths in a fuel cell segment [2] . . . . .	19
2.15	Schematic diagram of traditional serpentine [8] . . . . .	20
3.1	Simulink model overview . . . . .	21
3.2	Specific Enthalpy of Oxygen . . . . .	23
3.3	Model of $U_{chemical}$ . . . . .	24
3.4	Polarization Curves . . . . .	24
3.5	Heat loss . . . . .	25
3.6	Cooling system overview . . . . .	26
3.7	Heat exchange subsystem . . . . .	27
3.8	Parameters values . . . . .	28
3.9	Thermodynamic variables subsystem . . . . .	29
3.10	Focus on $\rho$ and $\alpha$ computation . . . . .	29
3.11	Nusselt number subsystem . . . . .	30
3.12	Grashof number computation . . . . .	31
3.13	Regime control block . . . . .	32
3.14	Moody diagram . . . . .	33

3.15	Heat exchange coefficient subsystem . . . . .	33
3.16	Pipes subsystem . . . . .	34
3.17	Centrifugal pump characteristic . . . . .	35
3.18	Pressure drop provided . . . . .	36
3.19	Experimental heat exchanged provided . . . . .	37
3.20	Experimental heat exchanged subsystem . . . . .	38
3.21	Radiator subsystem . . . . .	38
3.22	Output signal generated by control block . . . . .	39
3.23	Radiator control block . . . . .	40
3.24	Radiator control subsystem . . . . .	40
3.25	Coolant inflow subsystem . . . . .	41
3.26	Overview of the loop . . . . .	42
4.1	Current density from WLTP cycle . . . . .	44
4.2	Chemical voltage . . . . .	45
4.3	Cell voltage . . . . .	45
4.4	Heat loss . . . . .	46
4.5	Convective heat exchange coefficient . . . . .	47
4.6	Nusselt number . . . . .	47
4.7	Reynolds number . . . . .	48
4.8	Prandtl number . . . . .	48
4.9	Grashof number . . . . .	49
4.10	Friction factor . . . . .	49
4.11	Pressure drops comparison . . . . .	50
4.12	Mass flow rate . . . . .	50
4.13	Radiator heat exchange . . . . .	51
4.14	Stack temperature . . . . .	52
4.15	Focus on radiator starting time . . . . .	52
4.16	Example of how the radiator affects the temperature . . . . .	53
A.1	Nusselt number with friction factor and mass flow rate from Amesim	56
A.2	Convective heat exchange coefficient with friction factor and mass flow rate from Amesim . . . . .	57



# Chapter 1

## Introduction

In the current global energy issue, where decarbonization is required, many scientists see hydrogen as the fuel of the future in the post-fossil fuel era. Hydrogen could be a solution to one of the most challenging problems of renewables: discontinuous availability. In fact, it could play a fundamental role in long-term storage for those sources affected by the summer / winter cycle. Although hydrogen is not a source of energy and is not a readily available fuel, it could be an intermediate form of energy or an energy carrier. Just like electricity, hydrogen can be generated from a variety of energy sources, delivered to end users, and there converted into useful energy efficiently and cleanly.

In the transport sector hydrogen has some advantages over batteries: weight reduction is essential and high mileage with short refueling times is required. Hydrogen can be used in different applications such as heavy duty trailers and small airplanes.

Although it has many benefits, the main drawback is the lost of efficiency. The entire process requires two conversions: from electrical energy to hydrogen and back to electrical power. Today's technologies do not allow yet a high efficiency conversion.

### 1.1 Hydrogen for heavy-duty transport

Road transport, both of passengers and goods, accounts for 15% of  $CO_2$  emissions worldwide. Reducing  $CO_2$  emissions in this sector can have a major impact on the problem of global warming, even if it would not be enough. There are numerous practical reasons for developing a Hydrogen Fuel Cell System on these platforms.

In a FC there is more energy per unit mass than a lithium battery or diesel fuel. This difference amounts to more than two orders of magnitude. A truck can have, thus, a greater amount of power available with a insignificant increase of weight,

an important consideration for long-haul trucks that have weight penalties.

Hydrogen fuel cells are ideal for the trucking industry because the refueling time and driving range are comparable to diesel-powered trucks. Refueling time is higher but still on a similar order of magnitude with respect to diesel. This means that the charging stations can be occupied by several trucks at the same time.

To conclude, travel pathways are predictable, because trucks usually travel on dedicated routes. This implies a simplification for developing a fueling infrastructure, with a less diffused refueling stations network. [1]

## 1.2 Fuel Cells

A Fuel Cell (FC) is an electrochemical device that converts chemical energy directly into electrical energy. There are no intermediate passages into thermal energy and from that to mechanical one. The efficiency of a FC is thus not restricted to Carnot efficiency and it can achieve in principle 100% referring to lower heating value of reactants. As a matter of fact, this value is not reached but fuel cells may work at higher efficiency points than internal combustion engines and conventional power plants.

Because there is no combustion process in FCs, the only product of these devices is water and unused air. For this reason, fuel cell vehicles are considered as zero-emission vehicles if we were to consider only tailpipe emissions. Moreover, these devices are extremely simple, compact and modular but yet expensive because of materials costs.

There are many types of fuel cells, but in this dissertation Proton-Exchange Membrane (PEM) will be considered. In fact, they are particularly suitable for automotive applications because they:

- operate at low temperatures (maximum 90 °C);
- quick start-up;
- have high power density;
- have high safety with a solid electrolyte.

To sum up, fuel cells systems are a very promising technology for hydrogen utilization in transportation, capable of offering higher efficiency, zero tail emission, and at the same time low refueling time and weight. However, hydrogen must become a readily available commodity (not as a technical gas but as an energy carrier) before fuel cells can be fully commercialized. Moreover, some research about fuel cells is still required, especially in reliability and longevity, which are highly dependent on the temperature.

## **1.3 Aim of the work**

Considering the context, the aim of this work is to create a thermal model of a fuel cell system for an electric vehicle using Simulink. FC performance highly depend on operating conditions, in particular on temperature. For this reason, the heat generated cannot be neglected.

In this dissertation is first computed the heat generation. Then, is modelled the cooling system in order to refrigerate the FC. Finally, the results are compared with Simcenter Amesim to evaluate the predictability of the model.

## Chapter 2

# Fuel Cells and Cooling System

In this chapter a brief overview about fuel cells is provided. To further explore the subject, see [2][3][4].

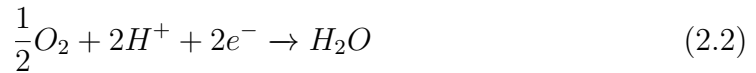
### 2.1 FC Working Principles

In a PEM fuel cell two electrodes are separated by a polymer membrane that does not conduct electrons but lets the positive ions pass. The electrons, finds them-self at a different electrical potential released by the chemical reaction, cross through an external electric circuit. In this way an electric current is produced by the fuel cell.

There are two semi-reactions that take place at the electrodes:  
At the anode the oxidation of hydrogen molecule occurs:



The positive ions pass through the protonic conductive membrane. While if no external circuit is present, the electrode becomes negatively charged.  
At the cathode oxygen reduces:



The two electrons are stripped from the electrode thus it becomes positively charged. Between the two charged electrodes an electric voltage is established. The overall reaction is:



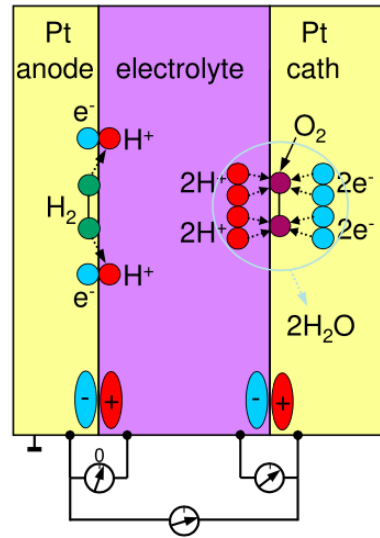


**Figure 2.1:** FC reaction principles [5]

## 2.2 FC Stack

A single hydrogen fuel cell is capable to provide only a theoretical voltage of approximately 1.2 V, which is lower when real application is considered. A stack is a multitude of cells connected in series in order to obtain a higher chemical voltage. A single fuel cell can be divided in two main parts:

- Bipolar Plates;
- Membrane Electrode Assembly (MEA), which includes Gas Diffusion Layer, Catalyst Layer and Electrolytic Membrane.

These components are analyzed in the next sections.

### 2.2.1 Bipolar Plates

Bipolar plates constitute the limit between two elementary cells and are the main mechanical structure support. The cell must withstand clamping force given by constraints and at the same time must be lightweight to have high power density. Bipolar plates have many other roles. They provide reactants to the cell through the gas channels to the diffusion layers ensuring the parting of reactive gases on either side. Plates must have, thus, low permeability. They must be either electrically conductive in order to collect electrons from one electrode (anode) to the other (cathode). This because bipolar plates are the element that electrically connect

the cells in series. Another role is to evacuate the unused gases, water and the heat generated during the chemical reaction. Heat is dissipated by the cooling channels. To do so, thermal conductivity must be as high as possible. To meet all the requirements in terms of material properties, bipolar plates are usually metallic or graphite-composite.

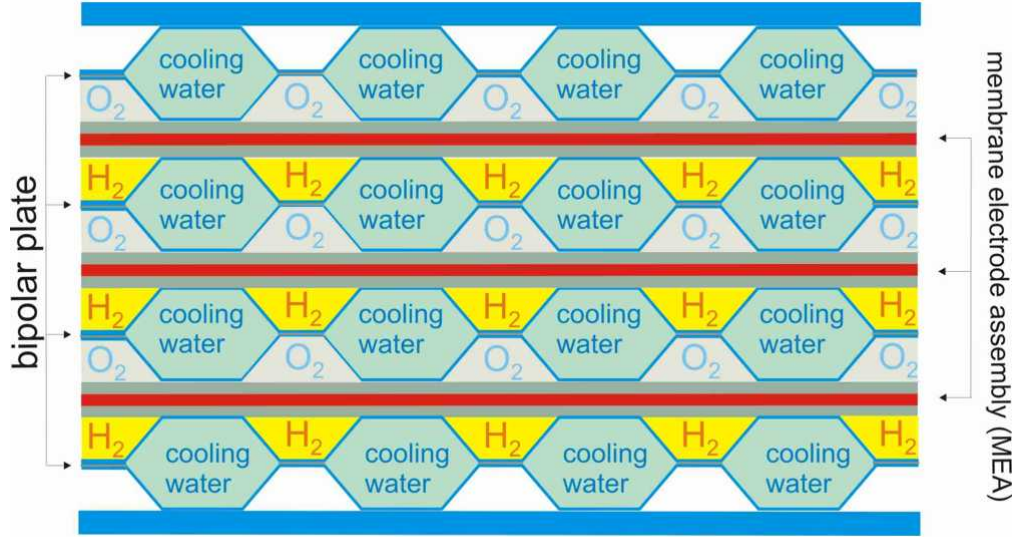


**Figure 2.2:** Bipolar plates scheme [6]

### 2.2.2 Gas Diffusion Layer

A fuel cell electrode is the layer where the oxidation of hydrogen and the reduction of oxygen take place. It consists of two zones: the gas diffusion layer and the catalyst layer.

The Gas Diffusion Layer (GDL) does not directly participate in the reaction but has the main function of providing the transit of reactants from the gas channels to the catalyst layer and vice versa for products. It also serves for closing the electrical circuit collecting electrons released in the reaction and conducting them to the bipolar plates. It conduct also the heat generated. To perform these functions GDL must be porous in both directions, electrically and thermally conductive, sufficiently rigid to support MEA. Carbon fiber-based materials fit the requirements, such as carbon paper or carbon cloth.

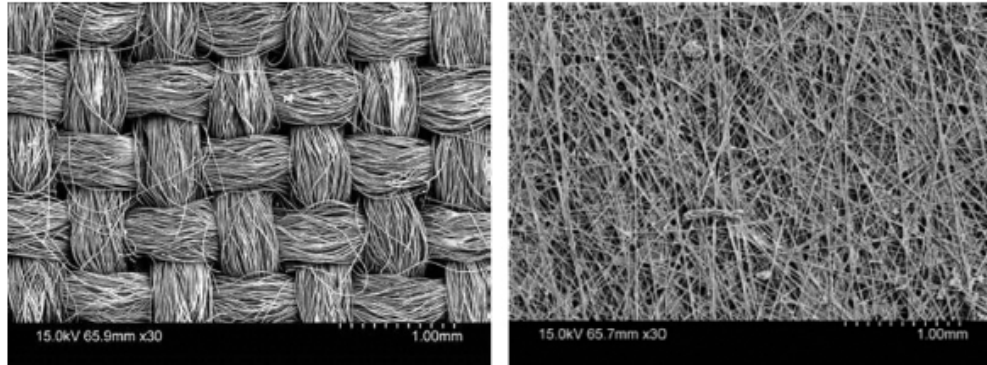


Figure 2.3: GDL carbon cloth on the left and carbon paper on the right [2]

### 2.2.3 Catalyst Layer

Catalyst layer is where electrochemical reactions occur. The most commonly used catalyst is Platinum. It can be directly applied on the membrane and then press the GDL on it or firstly on the GDL and then press the membrane. The function of catalyst layer is to promote the reaction by increasing the reaction rate.

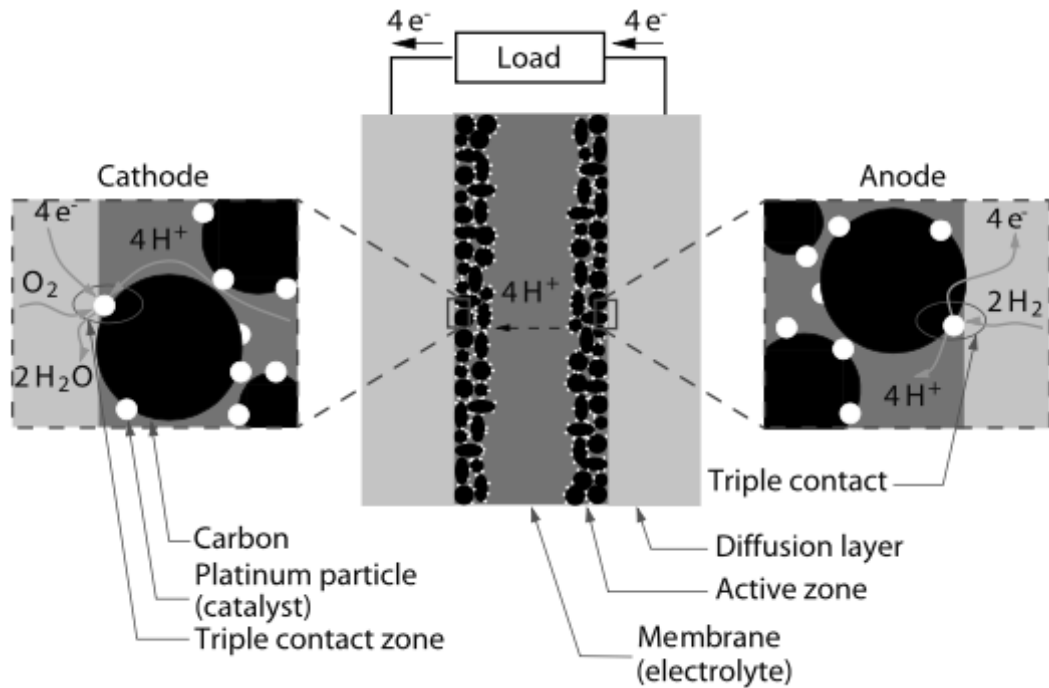


Figure 2.4: Catalyst layer structure [3]

## 2.2.4 Membrane

Membrane is a solid polymer that conduct proton from anode to cathode. It has to separate oxygen and hydrogen, so it must be proton conductive but also gas impermeable. The thickness of the membrane is a trade off of the two requirements.

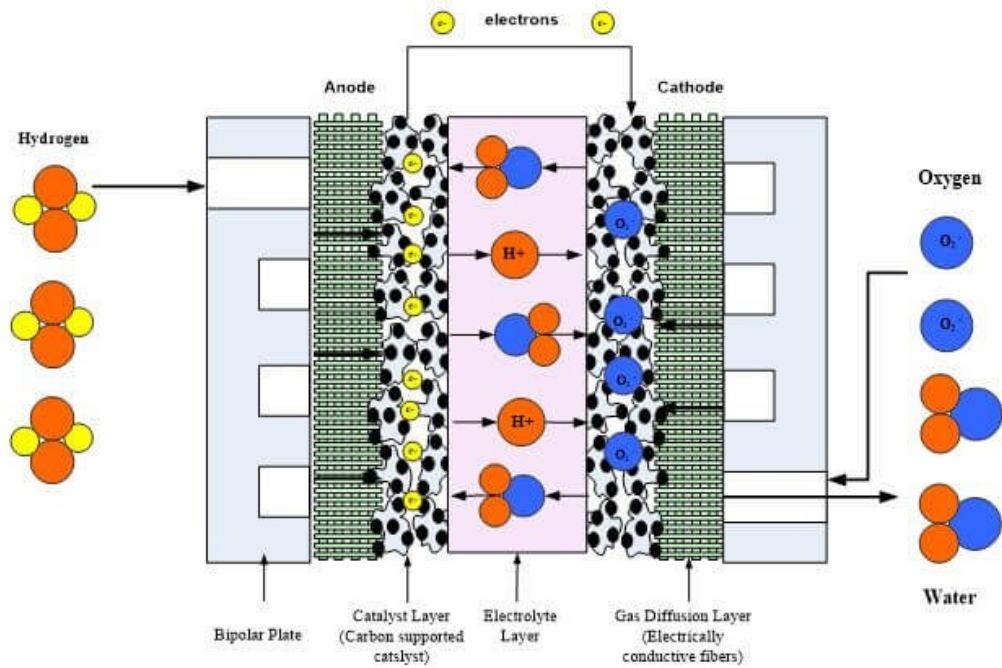
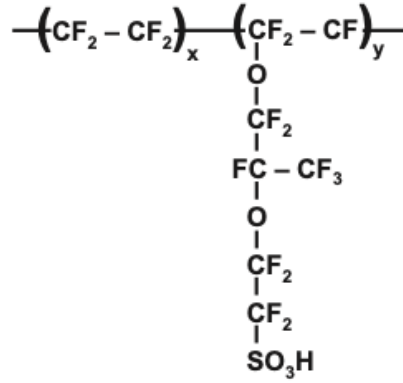


Figure 2.5: FC Overall functioning [7]

The material generally used is the Perfluorocarbon Sulfonic Acid (PFSA) ionomer known as Nafion<sup>TM</sup>. In figure 2.6 molecular structure of PFSA is shown. At the side of each chain there are  $SO_3^-$  and  $H^+$  ions. The protonic conductivity is given by the transit of the  $H^+$  ions. To guarantee it, membrane must be humid due to the hydrophilic behaviour of the  $SO_3H$  that absorbs a lot of water. Thus, membrane conductivity depends on the amount of humidity that depends on the temperature. PEM fuel cells operate therefore in a range between 25°C and 80°C.





**Figure 2.6:** Structure of PFSA [2]

## 2.3 Cell Voltage and efficiency

The total reaction of a cell is:



The heat released is given by the difference  $\Delta H$  between enthalpies of formation of reactants and products. The energy that can be converted into electricity is the one of Gibbs free energy

$$\Delta G = \Delta H - T\Delta S \quad (2.5)$$

Electrical work  $W_{el}$  is:

$$W_{el} = qE \quad (2.6)$$

where  $q$  is the total charge and  $E$  is the electric potential. This equation can be rewritten as:

$$W_{el} = n \cdot N_A \cdot q_{el} \cdot E = n \cdot F \cdot E \quad (2.7)$$

Total charge transferred to 1 *mol* of  $\text{H}_2$  is expressed as number of electrons  $n$  times Avogadro number  $N_A$  times electric charge of a single electron  $q_{el}$ . These last two factors are the Faraday's constant  $F$ .

Comparing free Gibbs energy and electric work it is obtained the theoretical fuel cell potential:

$$E_{th} = \frac{-\Delta G}{nF} = 1.23 \text{ V} \quad (2.8)$$

Because enthalpy and entropy depend on pressure and temperature, this value is correct only at 25 °C.

Theoretical efficiency is:

$$\eta = \frac{\Delta G}{\Delta H} \quad (2.9)$$

Another potential is defined and it is the maximum corresponding to the Low Heating Value (LHV) or High Heating Value (HHV):

$$E_{LHV} = \frac{-\Delta H}{nF} \quad (2.10)$$

By doing the ratio between the two potentials the expression of efficiency is obtained:

$$\eta = \frac{E_{th}}{E_{LHV}} = \frac{\frac{-\Delta G}{nF}}{\frac{-\Delta H}{nF}} = \frac{\Delta G}{\Delta H} \quad (2.11)$$

This expression demonstrates that efficiency depends on cell voltage and it is proportional to it.

## 2.4 Polarization curve

The theoretical cell voltage cannot actually reach the value of 1.23V because some unavoidable losses inside the fuel cell decrease the voltage. These losses are described in next section and are:

- Activation Losses: depending on electro-chemistry. They are also called over-potential and are necessary to allow the electro-chemical reaction.
- Internal Currents and Crossover Losses or Open Cell Voltage: depending on electrons and hydrogen molecules that cross the membrane.
- Ohmic Losses: depending on the ohmic resistance of membrane and conductors.
- Concentration Losses: depending on the diffusion mechanism.

The potential of one cell is the most crucial characteristic of a fuel cell, the polarization curve, and is defined as the theoretical voltage with a deduction of all the losses:

$$E_{cell} = E_{th} - E_{act} - E_{ohm} - E_{conc} - E_{OC} \quad (2.12)$$

The losses depend on the operational conditions of the fuel cell.

In order to plot the polarization curves, another parameter has to be delineate: the current density. It is defined as the current  $I$  per cell unit area  $A_{cell}$ :

$$i = \frac{I}{A_{cell}} \quad (2.13)$$

### 2.4.1 Activation Losses

A certain voltage difference from equilibrium is required to achieve the electrochemical reaction. This is called activation polarization and is associated with the stagnant kinetics of the electrode. The higher the exchange current density, the lower the activation losses. These losses occur both at the anode and at the cathode; however, oxygen reduction requires much higher overpotentials, which means a much slower reaction than hydrogen oxidation.

The Butler-Volmer equation defines activation losses in an implicit form:

$$i = i_0 \left( \exp \left[ \frac{-\alpha_{Rd} F (E_{act})}{RT} \right] - \exp \left[ \frac{-\alpha_{Ox} F (E_{act})}{RT} \right] \right) \quad (2.14)$$

with:

$E_{act} \rightarrow$  Activation Losses;

$i_0 \rightarrow$  exchange current density;

$F \rightarrow$  Faraday constant;

$\alpha_i \rightarrow$  charge transfer coefficient, an experimental parameter;

$R \rightarrow$  Gas constant;

$T \rightarrow$  Temperature.

A simplified way to show the activation losses is to use the so-called Tafel equation. It is an approximation of Butler-Volmer and shows activation losses in an explicit form:

$$E_{act} = \frac{RT}{\alpha F} \cdot \ln \left( \frac{i}{i_0} \right) \quad (2.15)$$

Figure 2.7 shows the behaviour of activation losses.

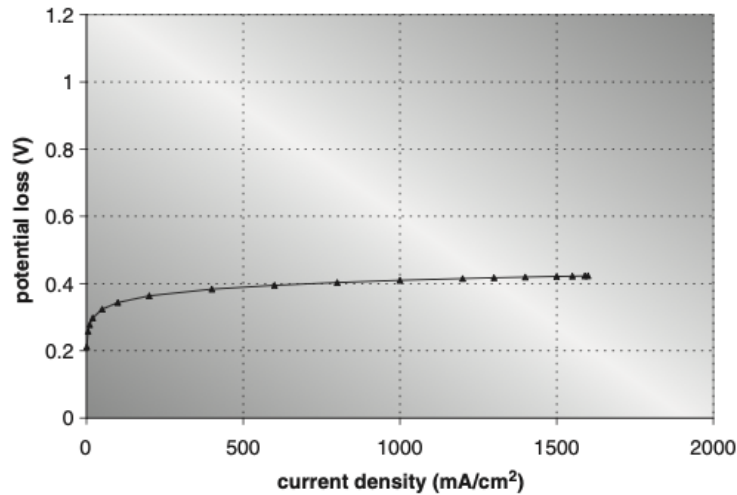


**Figure 2.7:** Voltage loss due to polarization activation [2]

The term  $\frac{RT}{\alpha F}$  is called Tafel slope and it depends solely on temperature and transfer coefficient. Thus, the higher the temperature the higher the activation losses.

### 2.4.2 Internal currents and crossover losses

These losses are related to electrons and hydrogen molecules that cross the membrane without contributing to electrical power. As a matter of fact, some of the hydrogen can diffuse through the membrane from the anode to the cathode, not supplying its electrons to the circuit. Similarly, a separate electron can pass through the membrane. This phenomenon can be described by an internal current to be added to the external current:

$$i = i_{ext} + i_{int} \quad (2.16)$$

Using Tafel equation and imposing  $i_{ext} = 0$ , with no external load, activation losses do not contribute anymore and currents and crossover losses can be evaluated:

$$E_{OCV} = \frac{RT}{\alpha F} \cdot \ln\left(\frac{i_{ext}}{i_0}\right) \quad (2.17)$$

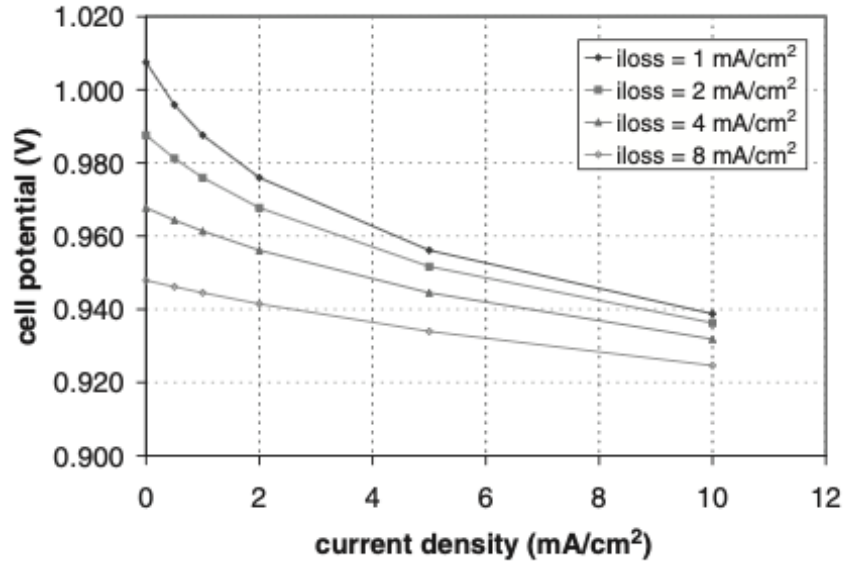


**Figure 2.8:** Effect of internal currents and/or hydrogen crossover loss on open circuit potential [2]

### 2.4.3 Ohmic losses

The ohmic losses occur due to the resistance imposed on the electrons by the conductive medium and the resistance of the electrolyte to the ions. The conductor resistance is actually lower than the membrane resistance, so the former is neglected. The ohmic resistance strongly depends on the number of molecules that there are inside the polymer membrane.

The voltage loss is the product between the current and the Membrane resistance  $R_m$ :

$$E_{ohm} = R_m i \quad (2.18)$$

The membrane resistance is obtained by integrating the conductivity over the membrane thickness  $t_m$ :

$$R_m = \int \frac{dz}{\sigma(T_{cell})} \quad (2.19)$$

with conductivity dependant on temperature:

$$\sigma(T_{cell}) = \exp \left[ 1268 \left( \frac{1}{303} - \frac{1}{273 + T_{cell}} \right) \right] \cdot \sigma_{30} \quad (2.20)$$

Figure 2.9 shows the behaviour of ohmic losses.

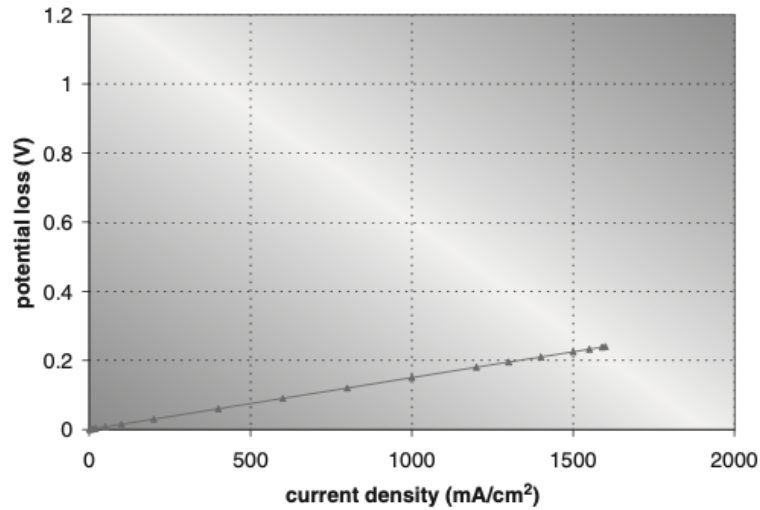
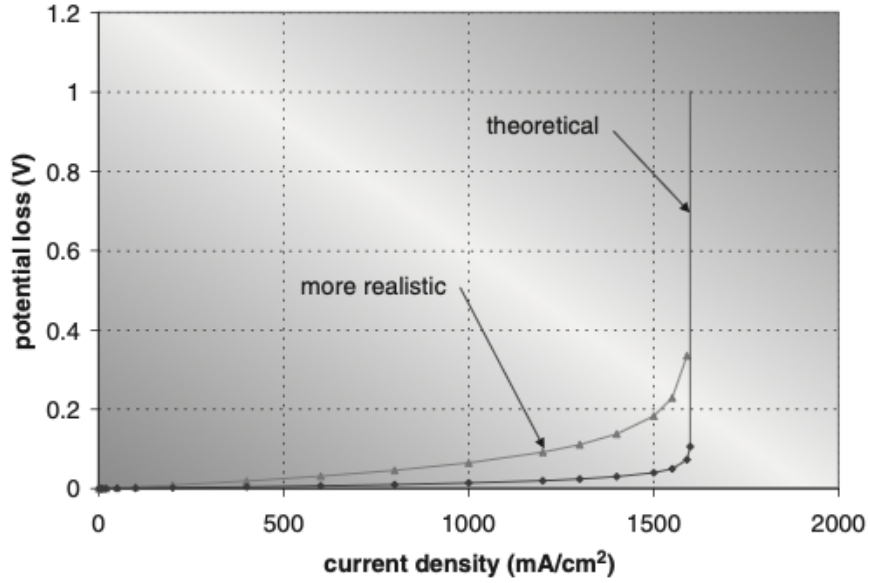


Figure 2.9: Resistive ohmic losses in the fuel cell [2]

### 2.4.4 Concentration losses

According to Faraday's law, at high currents, there is an increased rate of reactant consumption, which could be faster than diffusion through the diffusion layer. This

means a lower concentration of a reactant in the catalyst layer, with a voltage degradation. To quantify losses, one possibility is to calculate the pressure of the reactants in the catalyst layer, with a diffusion model. These types of models require information such as thickness, surface area, and diffusion coefficients of the gas diffusion layer. After calculating the pressure, this value is used to compute the theoretical voltage and activation losses.



**Figure 2.10:** Concentration polarization losses in the fuel cell [2]

Alternatively, it is possible to define a limiting current, at which the voltage drops to zero due to a lack of reactants in the catalyst layer. Considering Fick's law for one-dimensional diffusion:

$$N = \frac{D \cdot (C_B - C_S)}{\delta} A \quad (2.21)$$

Where:

$D \rightarrow$  Diffusion coefficient

$C_B \rightarrow$  Bulk concentration in gas channels

$C_S \rightarrow$  Catalyst Surface concentration

$\delta \rightarrow$  diffusion distance

In the steady state the rate of the consumed reactant is equal to the diffusion  $N = I/nF$ . Comparing the two equations:

$$i = \frac{nf \cdot D \cdot (C_B - C_S)}{\delta} \quad (2.22)$$

The limiting current is obtained by setting the concentration on the catalyst surface equal to zero,  $C_S = 0$ :

$$i_L = \frac{n f \cdot D \cdot (C_B)}{\delta} \quad (2.23)$$

By substituting in Nernst equation, the concentration losses are defined as:

$$E_{conc} = \frac{RT}{\alpha F} \cdot \ln\left(\frac{i_L}{i_L - i}\right) \quad (2.24)$$

### 2.4.5 Polarization curves

After defining the losses in fuel cell, it is possible to evaluate polarization curve. It is constituted by the theoretical potential minus the losses. Anode and cathode activation losses are grouped but the most of the losses occur at the cathode where oxygen reduction is slow.

As shown in figure 2.11, three different areas can be distinguished.

- Initial voltage drop: activation and internal currents losses prevail.
- Linear behaviour: in this sector ohmic losses are the most influential ones.
- Suddenly voltage drop: concentration losses and lack of reaction combine. In this window, the power loss is much higher than useful power. For this reason, it is a region where fuel cells should never work.

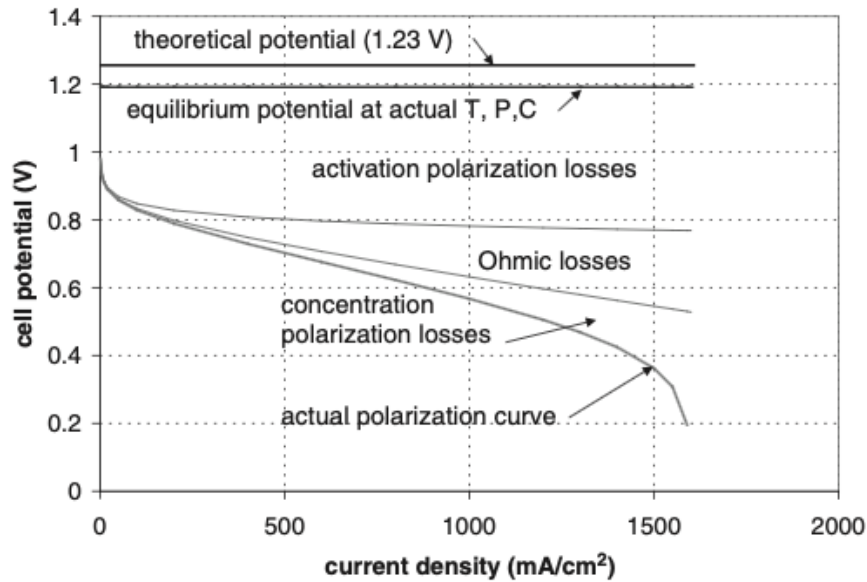


**Figure 2.11:** Voltage losses in the fuel cell and the resulting polarization curve [2]

Because the efficiency of a fuel cell is proportional to cell voltage, the efficiency curve has the same trend of polarization curve. Moreover, by multiplying cell voltage by the current, it is possible to obtain the useful power.

To sum up, polarization curves are fundamental because they represent the efficiency and the useful power of a fuel cell.

## 2.5 Effects of Temperature

The effect of operating temperature on fuel cell efficiency cannot be simply predicted from the equations that derive the polarization curve. Because temperature appears explicitly and implicitly in each voltage loss, in some cases the increase in temperature can lead to a efficiency gain and in others to a efficiency loss. The increase in temperature affects negatively efficiency because:

- the theoretical potential decreases, see equation 2.8 where  $T$  is contained in free Gibbs energy;
- Tafel slope increases leading to more losses.

On the other hand, higher temperature has positive effects on:

- exchange current density;
- ion conductivity;
- mass transport properties;
- gases have greater amounts of water vapor, reducing the chances of flooding with liquid water.

In conclusion, the performance of fuel cells usually improves with high temperatures, but only up to a certain threshold, depending on construction and operating conditions of the fuel cell.

Figure 2.12 shows the results of an experiment where temperature rises from  $-10\text{ }^{\circ}\text{C}$  to  $60\text{ }^{\circ}\text{C}$  with a clear voltage, and thus efficiency, gain.



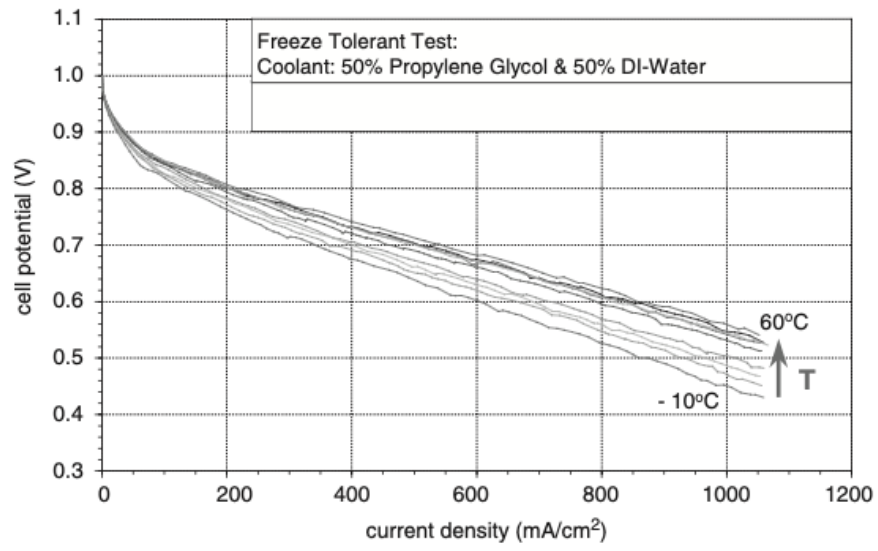


**Figure 2.12:** Effect of operating temperature on fuel cell polarization curve [2]

## 2.6 Cooling system

In general, the thermal and water management of PEMFCs are the most challenging issues in their implementation in vehicles. In fact, there is no exhaust phase, as in internal combustion engines, where most of the heat is dissipated and only a cooling system can manage the temperature of the stack. PEMFCs are generally handled within  $60 - 80\text{ }^{\circ}\text{C}$ . The high operating temperature levels of PEMFC stacks could significantly intensify membrane and catalyst degradation and thus reduce stack performance. To maintain the desired range inside the cells, the heat generated by the electrochemical reactions must be taken away. Different heat management schemes may be applied, such as:

- *Cooling with coolant flowing between the cells.* Coolant can be deionized water, antifreeze coolant, or air. Cooling is arranged between each cell, between each pair of cells, or between a group of cells (only for low-power densities because of higher temperatures in the center cells). Equal distribution of coolant can be obtained by having an arrangement similar to that of reactant gases.
- *Cooling with coolant at the edge of the active area (with or without fins).* The heat flows through the bipolar plate and then transfers to the refrigerant, typically air. The bipolar plate must be a very good thermal conductor to achieve relatively uniform temperature. Moreover, fins may need to be employed. This method results in a simpler stack, but it has heat transfer limitations.
- *Cooling with phase change.* Coolant is water or another phase-change medium. The stack design is simplified because water is already used in both anode and cathode area.

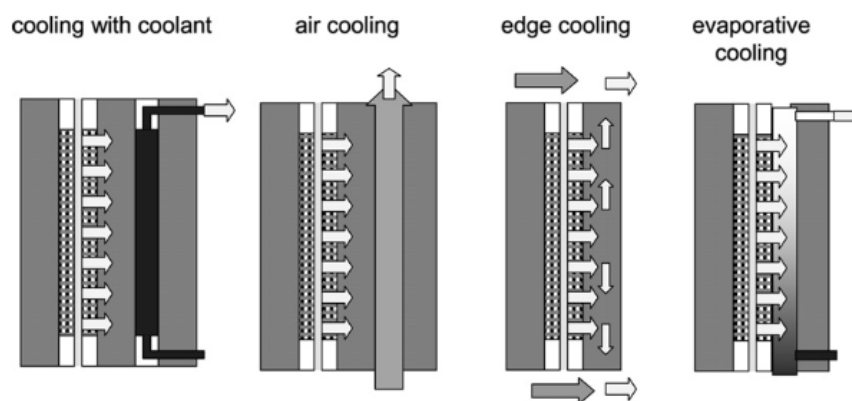


Figure 2.13: Different cooling options [2]

Cooling methods depend on several factors, such as the size of the FC, the complexity of the system, the application, the cost and the amount of heat recovered. For automotive applications and large vehicles, liquid cooling is preferred because it has no limitations in terms of size, weight and system complexity. In addition, liquid cooling has a high heat removal rate due to the high thermal conductivity and heat capacity. [8]

### 2.6.1 Stack heat balance

A complete stack energy balance takes into account many phenomena:

$$\sum Q_{in} = W_{el} + \sum Q_{out} + Q_{dis} + Q_c \quad (2.25)$$

with:

$Q_{in} \rightarrow$  enthalpy of reactant gases in;

$W_{el} \rightarrow$  electricity generated;

$Q_{out} \rightarrow$  enthalpy of unused reactant gases including heat of product water

$Q_{dis} \rightarrow$  heat dissipated to the surrounding

$Q_c \rightarrow$  heat taken away from the stack by active cooling.

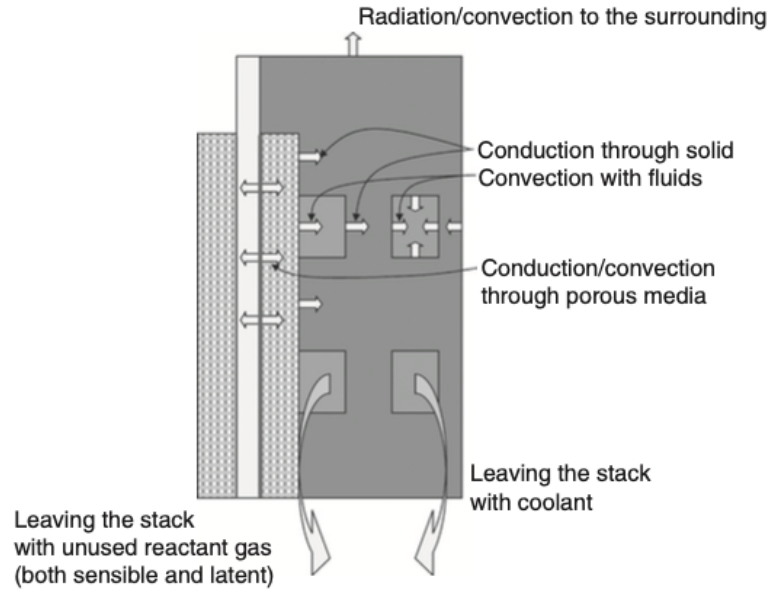


**Figure 2.14:** Heat paths in a fuel cell segment [2]

Most of the heat is generated in the catalyst layers, where losses are higher, predominantly on the cathode side. This heat is first carried by heat conduction through solid parts of the fuel cell. From equation 2.25 it is possible to notice that

some heat is transferred to the reactant gases (if their temperature is lower), some is transferred to the cooling fluid through forced convection, and some is conducted to the edge of the stack, where it is transferred to the surrounding air through radiation and natural convection.

### 2.6.2 Cooling systems

Generally, the cooling system is placed in the bipolar plates between anode and cathode. It is fundamental that the cooling medium has a low electrical conductivity because anode and cathode must be isolated to avoid efficiency losses. Conventional coolants with water and glycol mixture are too electrically conductive, either due to ion contamination from the bipolar plates or ionic production of the glycol. By adding antioxidants to them a low conductivity is maintained.

The cooling system must remove FC overheating by using the minimum pressure loss across the field and provide uniform temperature distribution by reducing the variations in the local temperature inside the active area of the FC. Literature has pointed out the importance of coolant channels design to improve the cooling performance. The most common designs are the parallel, serpentine, and parallel-serpentine, and each type has its unique feature. For further information refer to [8].

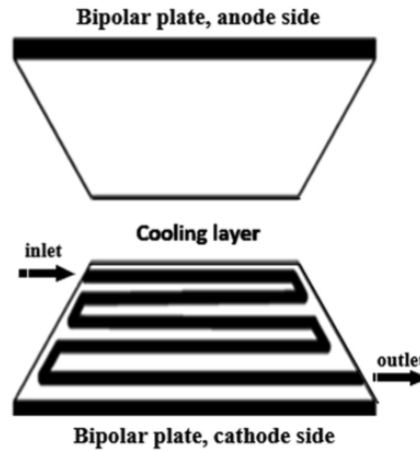


**Figure 2.15:** Schematic diagram of traditional serpentine [8]

## Chapter 3

# Simulink Model

To develop a thermal model of the Fuel Cell, Matlab/Simulink environment is chosen. Simcenter Amesim is taken as reference. In particular, Amesim provides a demo of a fuel cell system integration in a fuel cell electric vehicle. This demo illustrates how to model the complete fuel cell system including the cooling system. [9]. In Simulink model two subsystems are well defined:

- the first one where the fuel cell stack is designed and the heat produced is computed;
- the second where the cooling system is modelled;

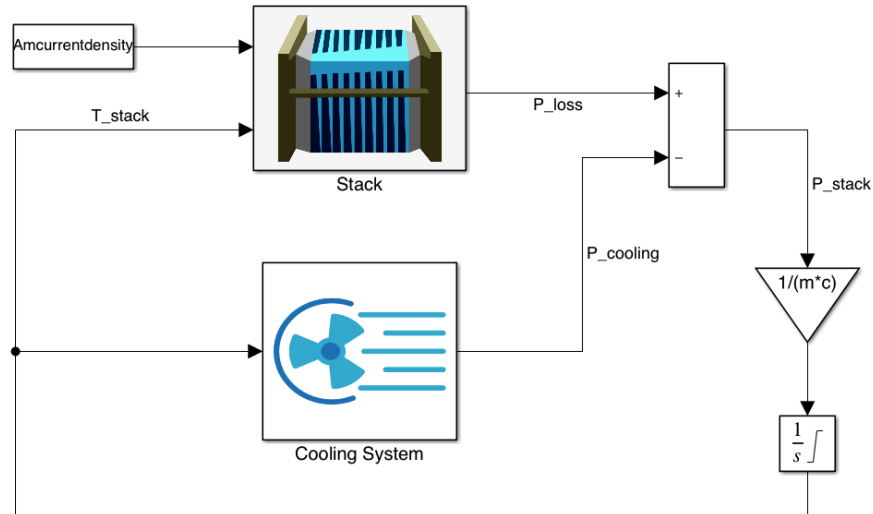


**Figure 3.1:** Simulink model overview

The output of both the two subsystems is heat power: from the heat dissipated by the stack is subtracted the power absorbed by the cooling system. This difference is the quantity absorbed by the stack heat capacity and contributes at its temperature increase; integrating this difference allow to compute the effective temperature of the fuel cell.

### 3.1 Stack

In this dissertation the modelling of the stack concerns only the heat losses and the efficiency of the fuel cell. Therefore, the calculations about voltage losses, seen in 2.4, are not included and the polarization curves are experimentally provided. The calculation of the heat generated by the stack is the main goal. It is described by the following equation:

$$P_{loss} = (U_{chemical} - U_{cell}) \cdot I_{stack} \cdot N_{cell} \quad (3.1)$$

where:

$U_{chemical} \rightarrow$  chemical voltage;

$U_{cell} \rightarrow$  cell voltage;

$I_{stack} \rightarrow$  output stack current;

$N_{cell} \rightarrow$  number of cells in the stack.

The geometric parameters of the stack are known. It has 330 *cells* and 400  $cm^2$  area. Its mass is equal to 50 *kg* and its specific heat is 1200  $\frac{J}{kgK}$ .

#### 3.1.1 Chemical voltage

The  $U_{chemical}$  is the potential corresponding to reactants' higher heating value. It is defined as a sum of:

$$U_{chemical} = U_{stat,c} + U_{stat,a} \quad (3.2)$$

The electro-static potential induced by species at cathode  $U_{stat,c}$  and that induced at anode  $U_{stat,a}$  are given by:

$$U_{stat,c} = - \left( \frac{M_{H_2O} \cdot h_{spec,H_2O}(P_c, T)}{2F} - \frac{M_{O_2} \cdot h_{spec,O_2}(P_c, T)}{4F} \right) \quad (3.3)$$

$$U_{stat,a} = \frac{M_{H_2} \cdot h_{spec,H_2}(P_a, T)}{2F} \quad (3.4)$$

with:

$M_i \rightarrow$  molar mass of the species *i*;

$h_{spec,i} \rightarrow$  specific enthalpy function of stack temperature  $T$  and pressure at the electrode  $P_j$ ;

$F \rightarrow$  Faraday's constant.

Molar mass can be easily taken from the periodic table, Faraday's constant is known, specific enthalpy must be calculated. NASA provides a polynomial formulation and the coefficients for each species [10]:

$$h_{NASA}(T) = r \cdot \left( -\frac{\alpha_1}{T} + \alpha_2 \cdot \ln(T) + \alpha_3 \cdot T + \frac{\alpha_4}{2} \cdot T^2 + \frac{\alpha_5}{3} \cdot T^3 + \frac{\alpha_6}{4} \cdot T^4 + \frac{\alpha_7}{5} \cdot T^5 + \alpha_8 \right) \quad (3.5)$$

with specific gas constant  $r$  defined as:

$$r = \frac{R}{M} \quad (3.6)$$

where  $R$  is the universal gas constant and  $M$  the molar mass. Pressure is not taken into account because a semi-real gas approach has been chosen. Figure 3.2 shows the specific enthalpy of oxygen; the operating time in which the NASA relationship is applicable is 200 – 1000K.

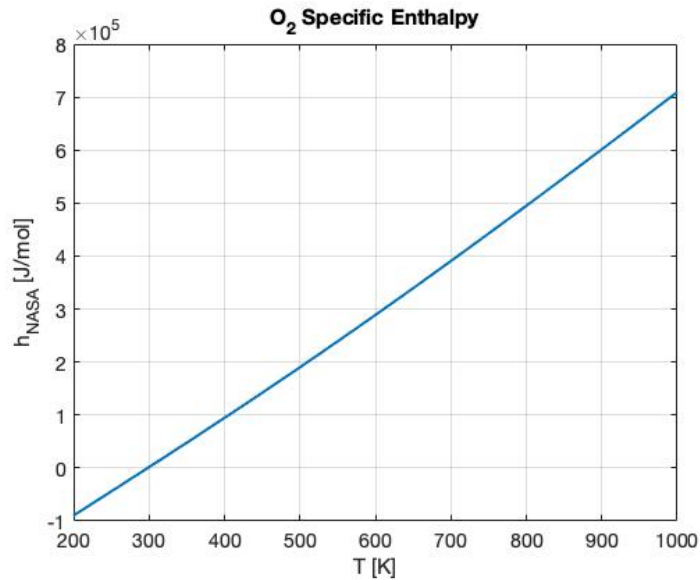


**Figure 3.2:** Specific Enthalpy of Oxygen

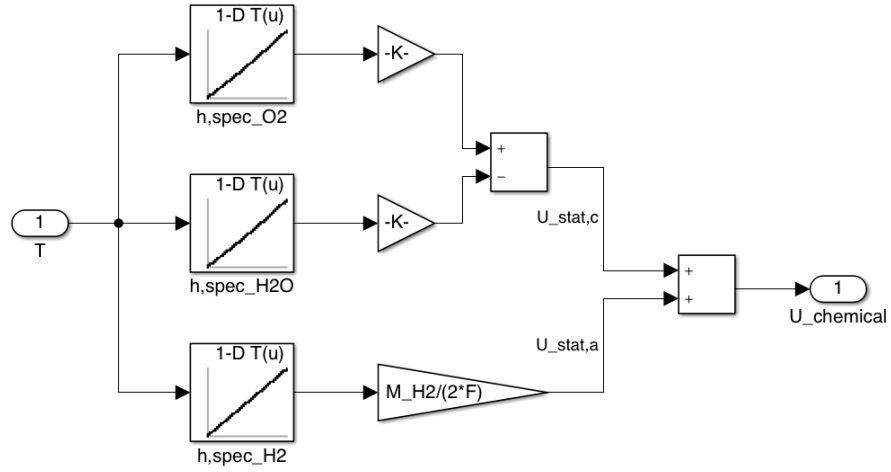


**Figure 3.3:** Model of  $U_{chemical}$

### 3.1.2 Cell Voltage

The cell voltage  $U_{cell}$  can be obtained through polarization curves. Amesim provides three curves at three different temperatures. Entering in the Simulink look-up table with stack temperature and current density, after an interpolation, it is possible to obtain the cell voltage. Current density is given as an input and it depends on the driving cycle chosen to simulate the model.

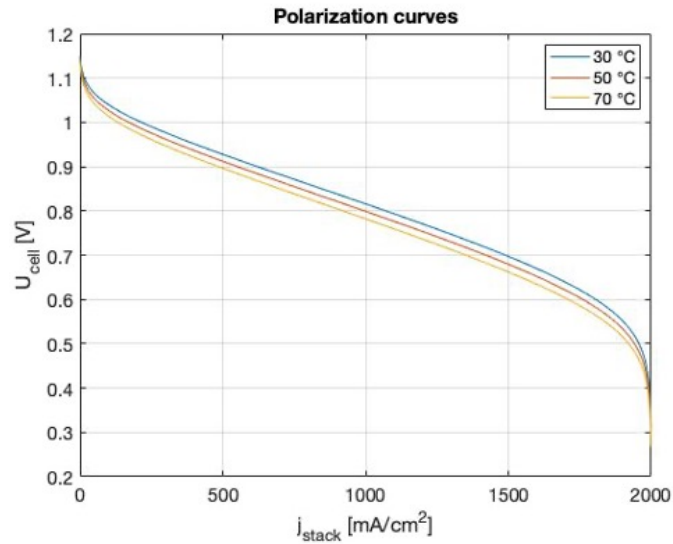


**Figure 3.4:** Polarization Curves



### 3.1.3 Heat loss

The difference between  $U_{chemical}$  and  $U_{cell}$  returns the voltage lost by each cell. To compute the total power lost  $P_{loss}$ , this value has to be multiplied by the total number of cells  $N_{cell}$ , that is a given value, and by the current  $I_{stack}$ . It is the current required to power the vehicle and it is obtained by multiplying the current density by the total area of the stack.

Figure 3.5 shows the stack power loss and, therefore, the entire stack.

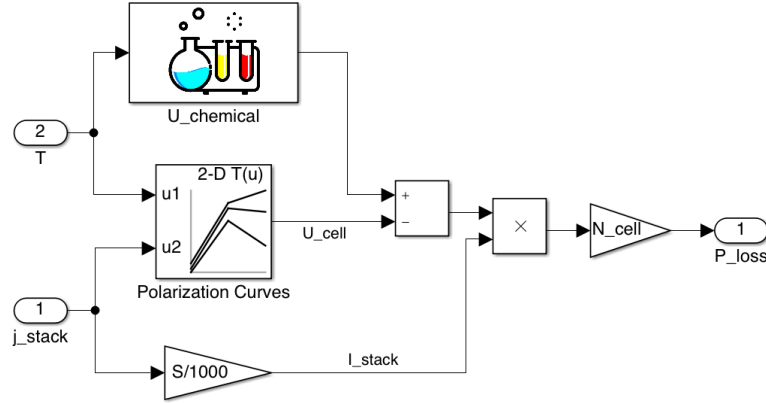


**Figure 3.5:** Heat loss

Once obtained the power loss, it is divided by the fuel cell mass and the heat capacity and then integrated to finally obtain the stack temperature  $T_{stack}$ .

## 3.2 Cooling System

The cooling system is a fluid dynamic circuit. A centrifugal pump generates the coolant flow in the cooling loop. Then the fluid exchanges heat with the stack. When the temperature rises above a threshold value a fan starts in order to exchange more heat with the radiator.

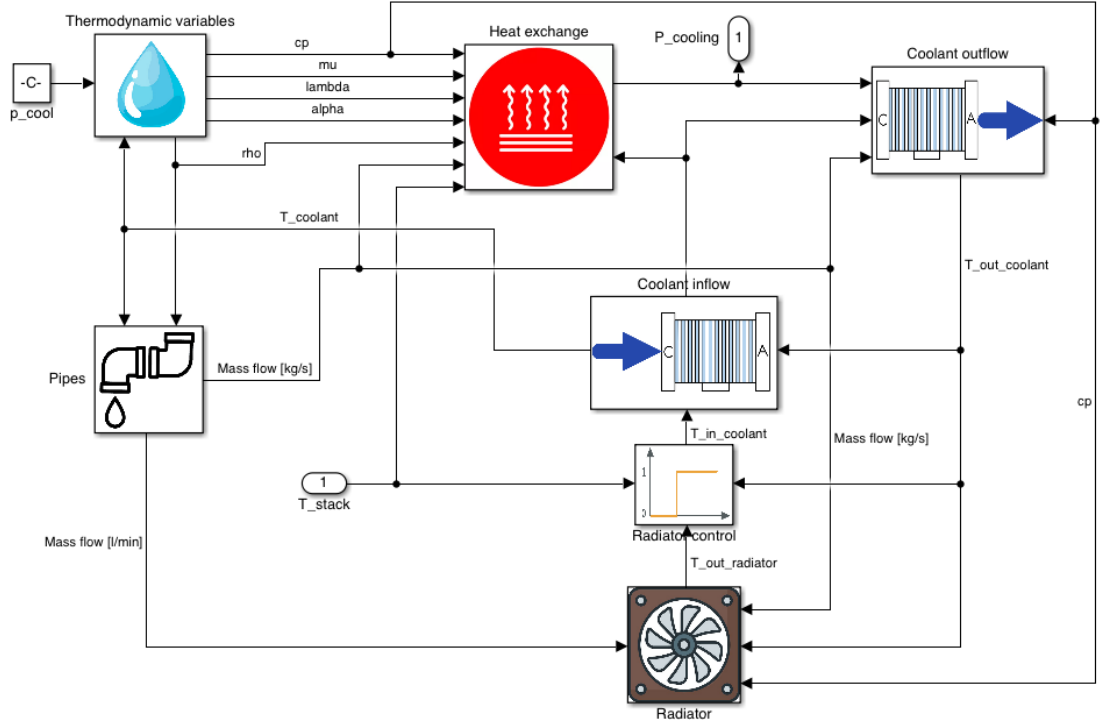


Figure 3.6: Cooling system overview

### 3.2.1 Heat exchange

The heat exchanged  $P_{cooling}$  [W] is computed with the first principle of thermodynamics. In our model is expressed with a Newton's law of cooling, as:

$$P_{cooling} = h_{conv} \cdot k_{heat} \cdot ce_{area} \cdot (T_{stack} - T_{coolant}) \quad (3.7)$$

$h_{conv}$  is the heat exchange coefficient for forced convection. It is analyzed in next section.

$k_{heat}$  is a geometric factor and is set equal to 1 because the pipes considered have a generic geometry.

$ce_{area}$  is the convective heat exchange area, it is given and it is equal to  $2640 \text{ cm}^2$ .

$T_{stack}$  is the temperature of the stack while  $T_{coolant}$  is the medium temperature of the refrigerant. These two values are part of the loop, in particular  $T_{coolant}$  can be evaluated only after having modelled the radiator.

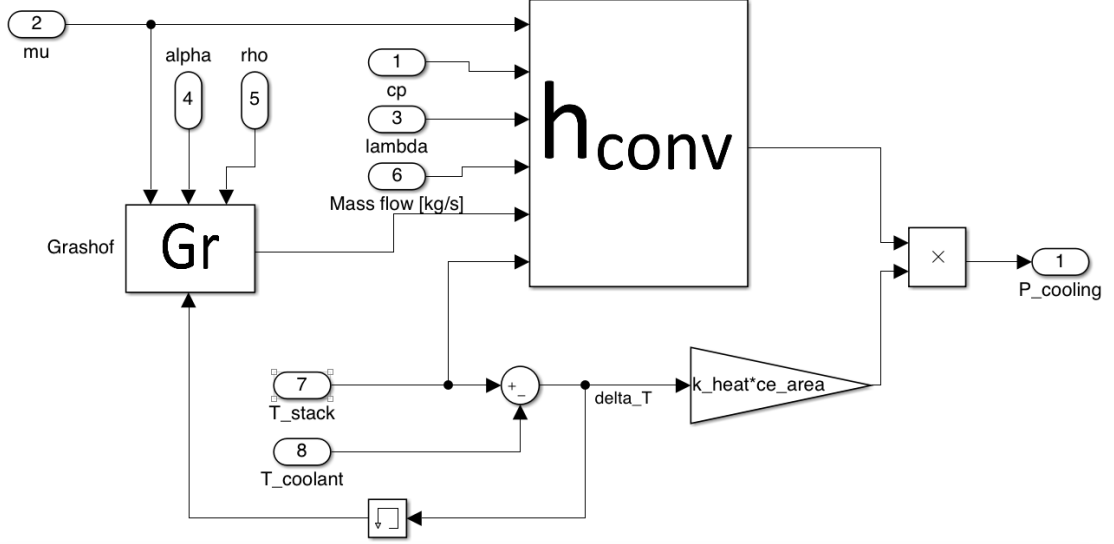


Figure 3.7: Heat exchange subsystem

### 3.2.2 Thermodynamic properties

Before analyzing the heat exchange coefficient, it is necessary to compute thermodynamic properties. The refrigerant is *EG60W40*: it is a solution of 60% of ethylene glycol in 40% of water.

All properties of the liquid are modelled by polynomials of the pressure and temperature. [11] Two polynomial models are available, the "simple" and the "advanced" one, the latter containing more monoms than the former one. The simple model is chosen. A special pressure value  $p_0$  and temperature value  $T_0$  is required for all properties and they are called "definition pressure" and "definition temperature".  $\Delta P = p - p_0$  denotes the difference between current and definition pressure and  $\Delta T = T - T_0$  denotes the difference between current and definition temperature. The fluid properties are now defined.

- Absolute viscosity [Pa.s]

$$\mu(p, T) = \mu_0 \cdot 10^{\chi(p, T)} \quad (3.8)$$

with:

$$\chi(p, T) = b_p \cdot \Delta p + b_t \cdot \Delta T + b_{t2} \cdot \Delta T^2 \quad (3.9)$$

- Specific heat  $[\frac{J}{kg \cdot K}]$

$$c_p(p, T) = c_{p0} \cdot [1 + c_t \cdot \Delta T + c_{t2} \cdot \Delta T^2 + c_p \cdot \Delta p + c_{pt} \cdot \Delta p \cdot \Delta T] \quad (3.10)$$

- Density  $[\frac{kg}{m^3}]$

$$\rho(p, T) = \frac{1}{v_s} \quad (3.11)$$

with:

$$v_s(p, T) = v_{s0} \cdot [1 + a_t \cdot \Delta T + a_p \cdot \Delta p + a_{pt} \cdot \Delta p \cdot \Delta T + a_{t2} \cdot \Delta T^2 + a_{p2} \cdot \Delta p^2] \quad (3.12)$$

- Volumetric expansion coefficient  $[\frac{1}{K}]$ , defined by Bode equation of state:

$$\alpha(p, T) = \frac{1}{v_s} \left( \frac{\partial v_s}{\partial T} \right) \bigg|_p \quad (3.13)$$

$$\alpha(p, T) = \frac{1}{v_s} \cdot v_{s0} \cdot [a_t + a_{pt} \cdot \Delta p + 2a_{t2} \cdot \Delta T] \quad (3.14)$$

- Thermal conductivity  $[\frac{W}{K \cdot m}]$

$$\lambda(p, T) = \lambda_0 \cdot [1 + d_t \cdot \Delta T + d_{t2} \cdot \Delta T^2] \quad (3.15)$$

The parameters are taken from the NIST online fluid database. [12]

$p_0$	Definition pressure	$1 \cdot 10^5$	[PaA]
$T_0$	Definition Temperature	$2 \cdot 10^1$	[°C]
$\rho_0$	Definition density	$1.075 \cdot 10^3$	[kg/m³]
$\mu_0$	Definition viscosity	$4.999 \cdot 10^3$	[kg/m/s]
$c_{p0}$	Definition specific heat	$3.100 \cdot 10^3$	[J/kg/K]
$\lambda_0$	Definition thermal conductivity	$3.890 \cdot 10^{-1}$	[W/m/K]
$a_t$	Temperature coeff. for specific volume	$5.984 \cdot 10^{-4}$	
$a_{t2}$	Squared temperature coeff. for specific volume	$1.723 \cdot 10^{-6}$	
$a_p$	Pressure coeff. for specific volume	$-1.250 \cdot 10^{-9}$	
$a_{pt}$	Pressure*temperature coeff. for specific volume	0	
$a_{p2}$	Squared pressure coeff. for specific volume	$7.812 \cdot 10^{-19}$	
$b_t$	Temperature coeff. for viscosity	$-1.745 \cdot 10^{-2}$	
$b_{t2}$	Squared temperature coeff. for viscosity	$8.789 \cdot 10^{-5}$	
$b_p$	Pressure coeff. for viscosity	0	
$c_t$	Temperature coeff. for specific heat	$2.065 \cdot 10^{-3}$	
$c_{t2}$	Squared temperature coeff. for specific heat	$-6.594 \cdot 10^{-6}$	
$c_{pt}$	Pressure*temperature coeff. for specific heat	$-1.034 \cdot 10^{-12}$	
$c_p$	Pressure coeff. for specific heat	$-3.031 \cdot 10^{-10}$	
$d_t$	Temperature coeff. for thermal conductivity	$-6.884 \cdot 10^{-4}$	
$d_{t2}$	Squared temperature coeff. for thermal conductivity	$-2.027 \cdot 10^{-6}$	

**Figure 3.8:** Parameters values

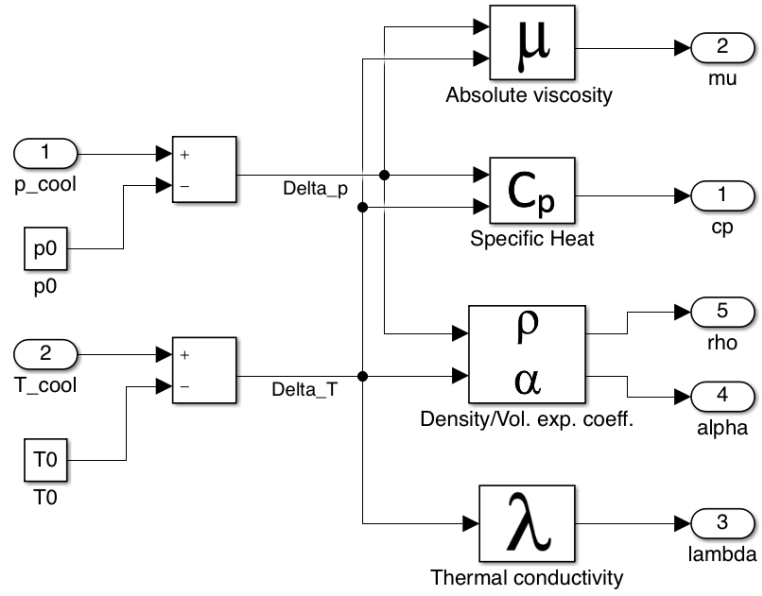


Figure 3.9: Thermodynamic variables subsystem

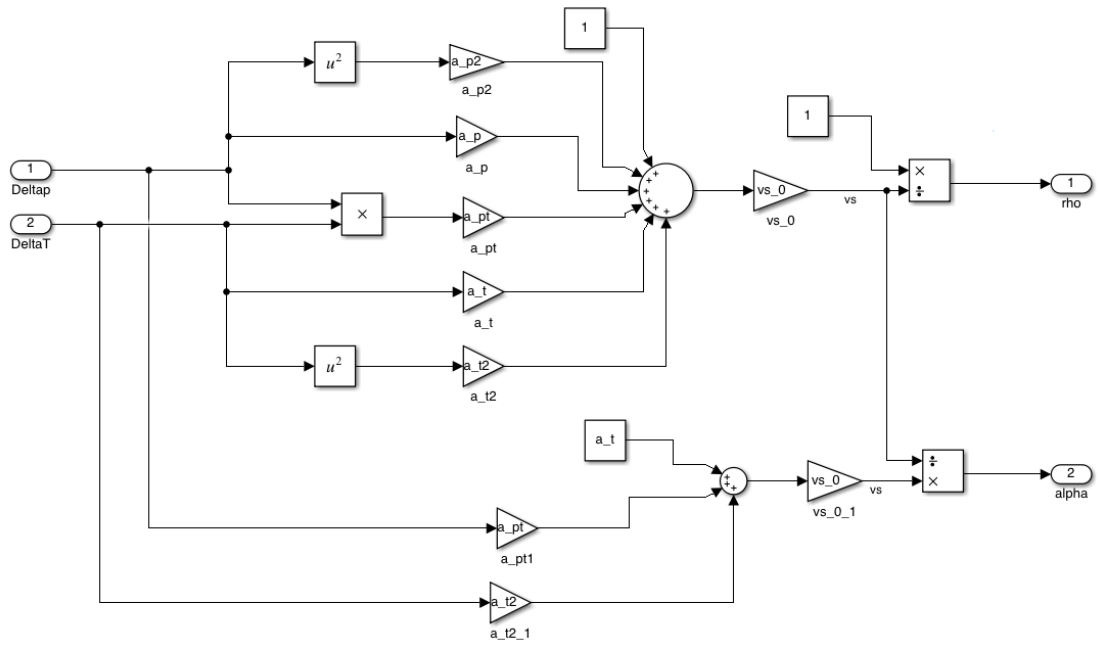


Figure 3.10: Focus on  $\rho$  and  $\alpha$  computation

### 3.2.3 Heat exchange coefficient

The heat exchange coefficient  $h_{conv}$  is computed as:

$$h_{conv} = \frac{Nu \cdot \lambda}{c_{dim}} \quad (3.16)$$

$\lambda$  is the thermal conductivity,

$c_{dim}$  is the characteristic length of heat exchange and is equal to 10 mm,

$Nu$  is the Nusselt number. It is defined as:

$$Nu = \sqrt[3]{Nu_{free}^3 + Nu_{forced}^3} \quad (3.17)$$

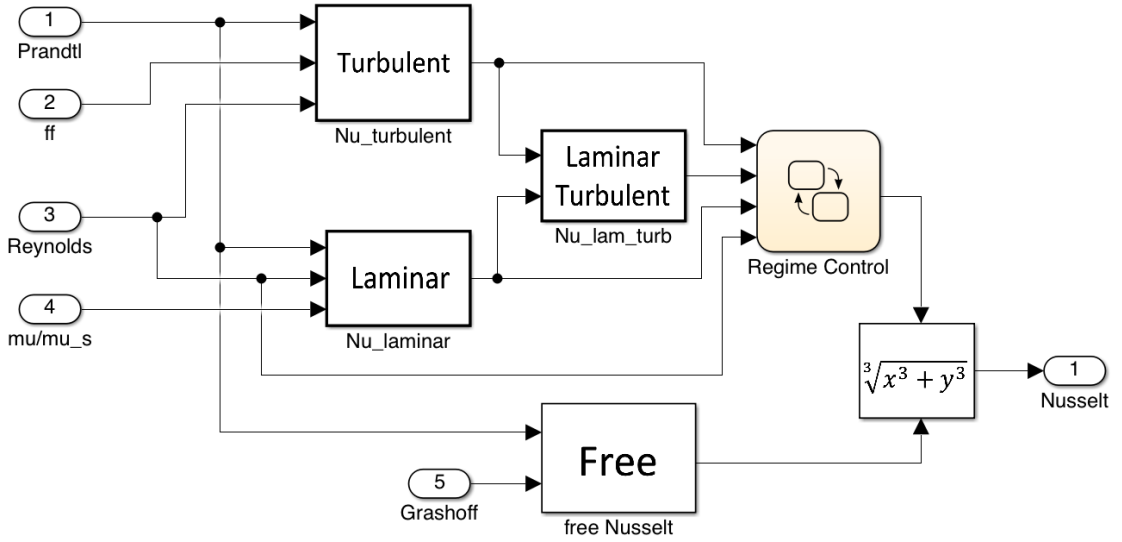


**Figure 3.11:** Nusselt number subsystem

The first term considers the free convection while the second considers forced convection between stack and refrigerant fluid.

- Expression for free Nusselt number is:

$$Nu_{free} = 0.53 \cdot \sqrt[3]{Gr \cdot Pr} \quad (3.18)$$

$Pr$  is the Prandtl number defined as:

$$Pr = \frac{\mu \cdot C_p}{\lambda} \quad (3.19)$$

$Gr$  is the Grashof number defined as:

$$Gr = \frac{c_{dim}^3 \cdot g \cdot \rho^2 \cdot \alpha \cdot (T_{stack} - T_{coolant})}{\mu^2} \quad (3.20)$$

$g$  is the gravity acceleration.

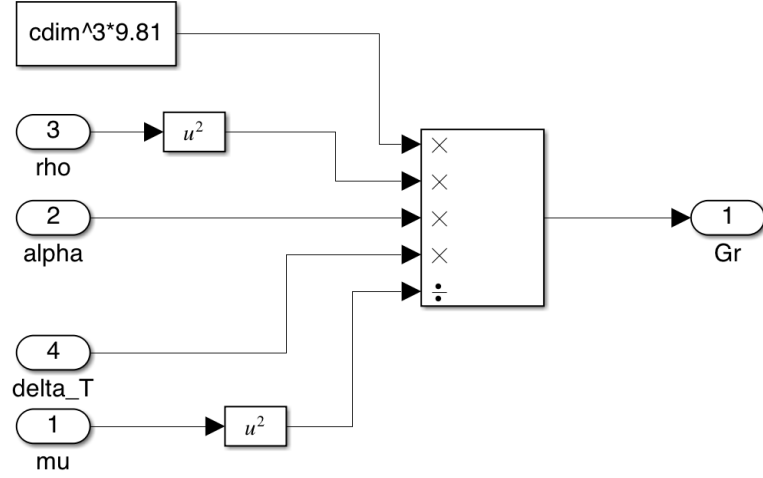


**Figure 3.12:** Grashof number computation

- Forced Nusselt is more difficult to be computed because it is necessary to know the regime of the fluid flow. In order to do so Reynolds number  $Re$  has to be known.

Reynolds number is computed as:

$$Re = \frac{dm \cdot c_{dim}}{\mu \cdot area} \quad (3.21)$$

$dm$  is the mass flow rate in  $\frac{kg}{s}$  and it is obtained from the pipes subsystem. It will be further analyzed in next section.

$area$  is the cross sectional area of the pipes, it is given and it is equal to  $30 \text{ mm}^2$ . It is now possible to define:

$$Nu_{forced} = \begin{cases} Nu_{lam} & \text{if } Re < Re_{trans1} \\ Nu_{turb} & \text{if } Re > Re_{trans2} \end{cases} \quad (3.22)$$

Therefore, if  $Re$  is smaller than  $Re_{trans1} = 2300$  the fluid is in laminar regime, if  $Re$  is higher than  $Re_{trans2} = 10000$  the fluid is in turbulent regime. If Reynolds stays between the two values the regime is laminar/turbulent and:

$$Nu_{lam/turb} = \sqrt{Nu_{lam}^2 + Nu_{turb}^2} \quad (3.23)$$

In order to make the model use the correct value of  $Nu$ , a control block from Stateflow is implemented. The block receives as inputs  $Nu_{lam}$ ,  $Nu_{turb}$ ,  $Nu_{lam/turb}$

and  $Re$ . By comparing the value of Reynolds with  $ReTrans1$  and  $ReTrans2$ , it switches state returning as output the correct value of Nusselt.

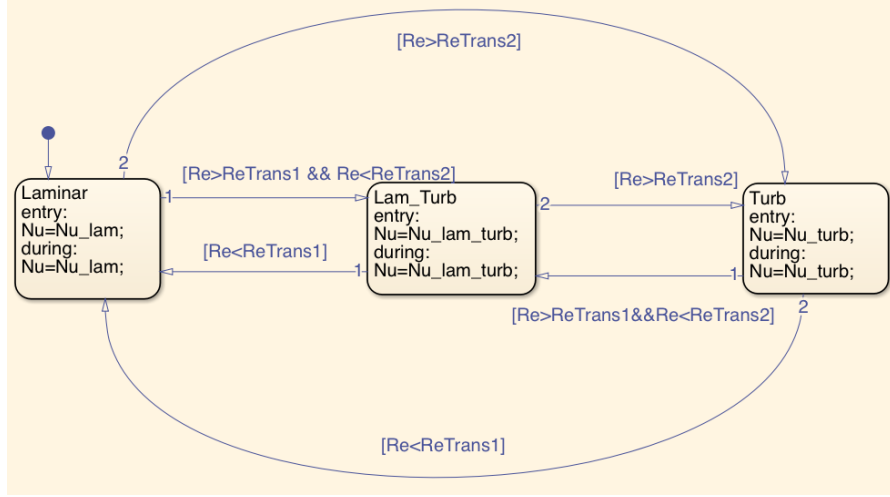


**Figure 3.13:** Regime control block

The expression for forced laminar Nusselt is defined from Sieder and Tate correlations [13]:

$$Nu_{lam} = 1.86 \cdot \left( \frac{Re \cdot Pr}{L/dh} \right)^{1/3} \cdot \left( \frac{\mu}{\mu_s} \right)^{0.14} \quad (3.24)$$

$L$  is the length of each cell channel and is set to 1 m;

$dh$  is the hydraulic diameter of the channels;

$\mu$  is the absolute viscosity in the pipe at coolant temperature while  $\mu_s$  is the absolute viscosity at stack temperature.  $\mu_s$  is computed such as in equation 3.8 with  $\Delta T = T - T_0$  referred to  $T_{stack}$ . The equation for forced turbulent Nusselt is:

$$Nu_{turb} = \frac{ff}{8} \cdot (Re - 1000) \cdot \frac{Pr}{1 + 12.7 \cdot \sqrt{\frac{ff}{8}} \cdot (Pr^{2/3} - 1)} \quad (3.25)$$

$ff$  is the friction factor obtained from moody diagram. The moody diagram is realized with a Matlab function block: relative roughness  $rr$  and Reynolds number enter the block, a Matlab function interpolates the Moody curves and finds the friction factor. Relative roughness chosen for the fuel cell is 10  $\mu m$ .



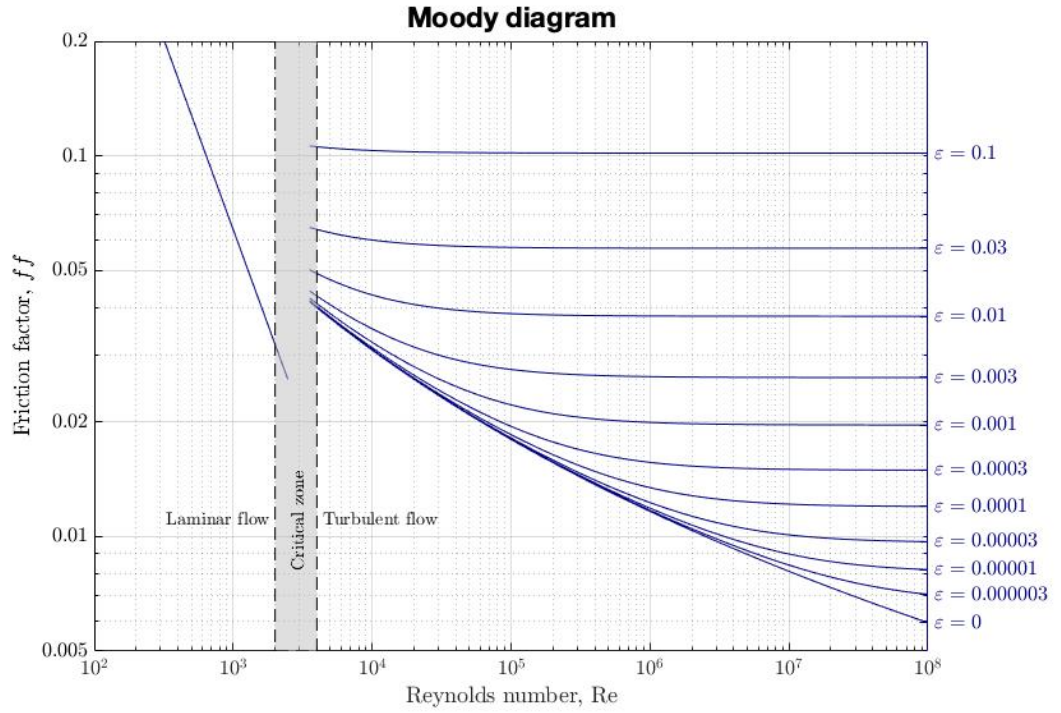


Figure 3.14: Moody diagram

The resulting model is shown in figure 3.15.

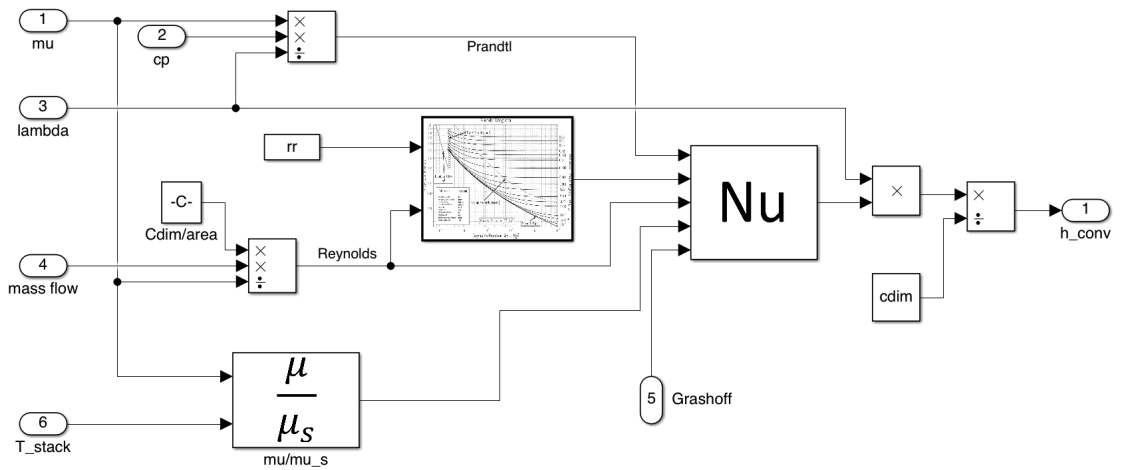
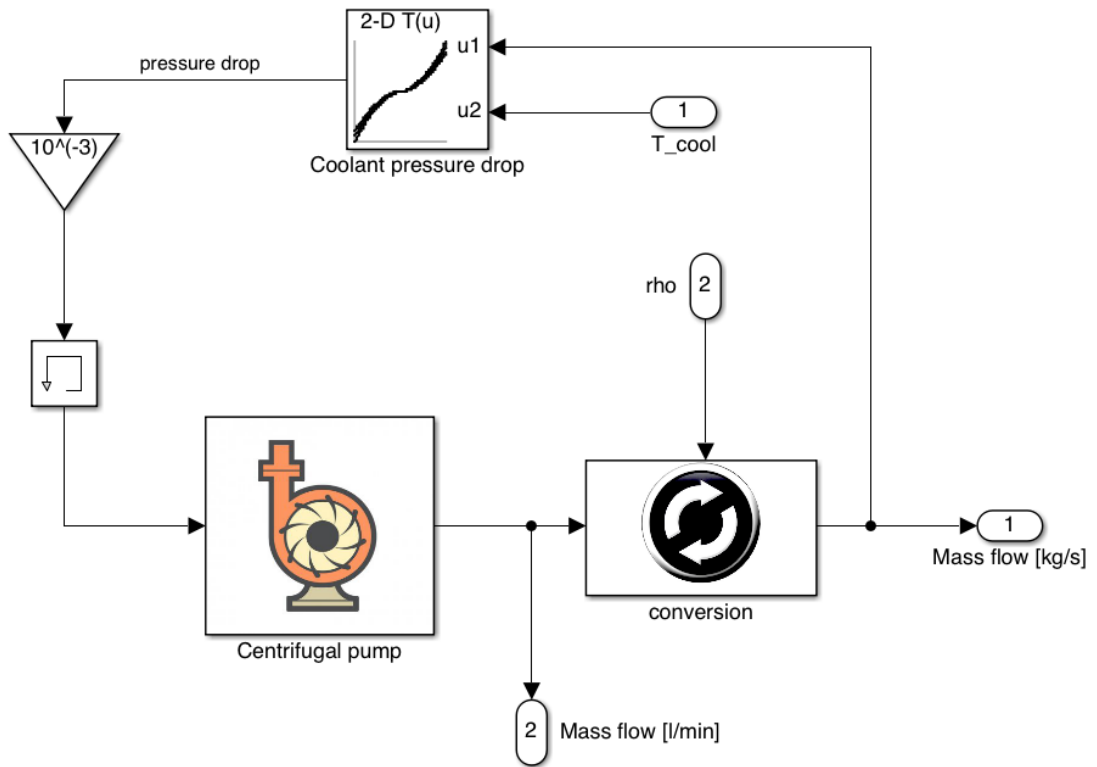


Figure 3.15: Heat exchange coefficient subsystem

### 3.2.4 Centrifugal pump and pressure drops

In this section the hydraulic aspect is analyzed. It is modelled as a loop initialized with a pressure drop set to 0. The only pressure drop considered is the one in the stack channels, while the one in pipes is assumed negligible. It must be pointed out that in this subsystem there is only a drop, therefore there is a relative pressure. The absolute pressure of the cooling system is set to 2 *bar* and it affects only thermodynamic variables.



**Figure 3.16:** Pipes subsystem

The centrifugal pump is modelled with a 2-D table that represents the characteristic curves of the pump. It requires as input the pressure drop and the number of rounds per minute *rpm*. This value can be changed to regulate the entire system. The higher the speed the higher the mass flow rate and so the heat taken from the stack.

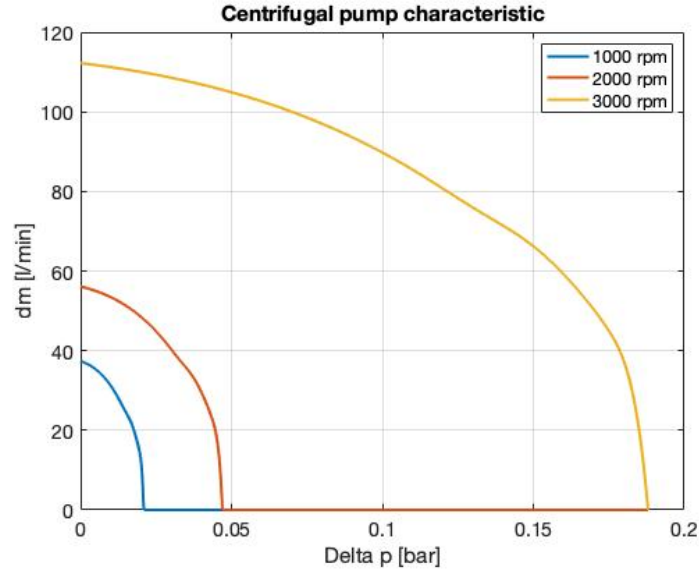


**Figure 3.17:** Centrifugal pump characteristic

The pump gives as output the mass flow rate  $dm$  in  $\frac{l}{min}$ . It is then converted in  $\frac{kg}{s}$  and is used both to compute Reynolds number and pressure drop. In fact, pressure drop in the stack is modelled with a 2-D table and depends on mass flow rate and temperature. The output  $\Delta P$  closes the loop.

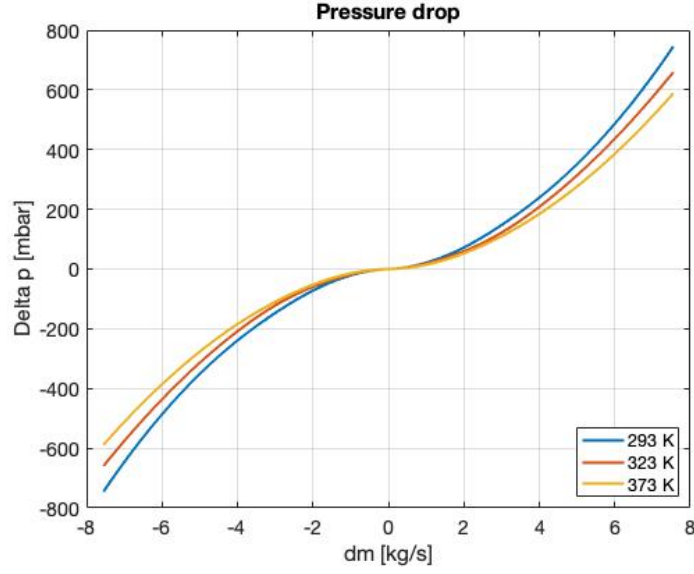


**Figure 3.18:** Pressure drop provided

### 3.2.5 Radiator

After having exchanged heat with the stack, the hot refrigerant enters the radiator. To compute the fluid temperature leaving the stack, first principle of thermodynamics is applied:

$$T_{out_{coolant}} = T_{in_{coolant}} + \frac{P_{cooling}}{c_p \cdot dm} \quad (3.26)$$

The heat exchanged between the coolant and the air passing through the radiator is a function of the coolant volumetric flow rate and the air velocity across the radiator. Air velocity  $V_{air_{rad}}$  is 15% of the vehicle speed. This reduction is attributed to the cooling duct opening: if the duct opening is made larger it increases the drag and hence a trade-off is made between the aerodynamic coefficient and the cooling performance. Vehicle speed is taken from the driving cycle given as input to test the entire model. The radiator has an integrated fan that can switch from off to on status. The operating of the fan induces an increase of the air velocity. The fan rotates in order to increase air speed of a value  $V_{fan}$  set to 4 m/s. The projected area of the fan on the radiator acts as the ventilated surface of the radiator. Hence, the velocity of air through the ventilated surface is:

$$V_{vs} = V_{air_{rad}} + V_{fan} \quad (3.27)$$

The geometric parameters of the radiator are known:

$D_{ext} = 30 \text{ cm}$  is the external of the fan;

$D_{int} = 0.5 \text{ cm}$  is the internal of the fan;  
 $R_h = 54.7 \text{ cm}$  is the radiator height;  
 $R_l = 41.5 \text{ cm}$  is the radiator length.  
 Area of the ventilated surface is:

$$A_{vs} = \frac{\pi}{4} \cdot (D_{ext}^2 - D_{int}^2) \quad (3.28)$$

The heat exchanged between the coolant and the air passing through the radiator is a function of the coolant volumetric flow rate  $q_{lh}$  and the air velocity across radiator. A 2-D table is given. It provides the experimental heat exchanged measured at a  $\Delta T_{exp}$  temperature difference of  $70 \text{ }^\circ\text{C}$ . The experimental heat exchanged on the ventilated surface is:

$$H_{V_{exp}} = f(V_{vs}, q_{lh}) \cdot \frac{A_{vs}}{R_h \cdot R_l} \quad (3.29)$$

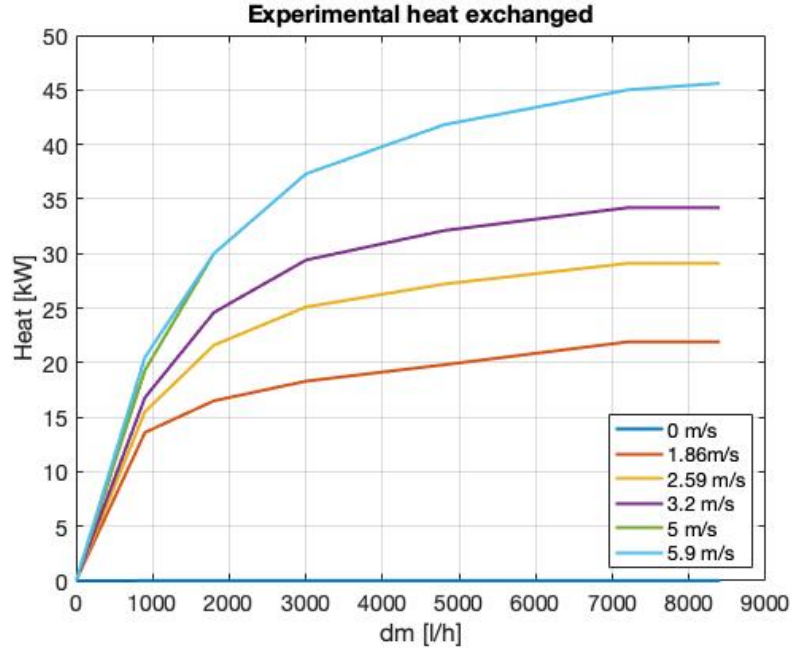


**Figure 3.19:** Experimental heat exchanged provided

The same passages are applied to the non-ventilated surface area  $A_{nvs}$  and heat exchanged  $H_{NV_{exp}}$ :

$$A_{nvs} = R_h \cdot R_l - A_{vs} \quad (3.30)$$

$$H_{NV_{exp}} = f(V_{air_{rad}}, q_{lh}) \cdot \frac{A_{nvs}}{R_h \cdot R_l} \quad (3.31)$$

The total experimental heat exchanged is then:

$$H_{exp} = H_{V_{exp}} + H_{NV_{exp}} \quad (3.32)$$

To compute the real heat exchanged the  $H_{exp}$  has to be scaled for the actual  $\Delta T$ :

$$H_{real} = H_{exp} \cdot \frac{T_{out_{coolant}} - T_{air}}{\Delta T_{exp}} \quad (3.33)$$

where  $T_{air}$  is the external air temperature and is set to 20 °C.

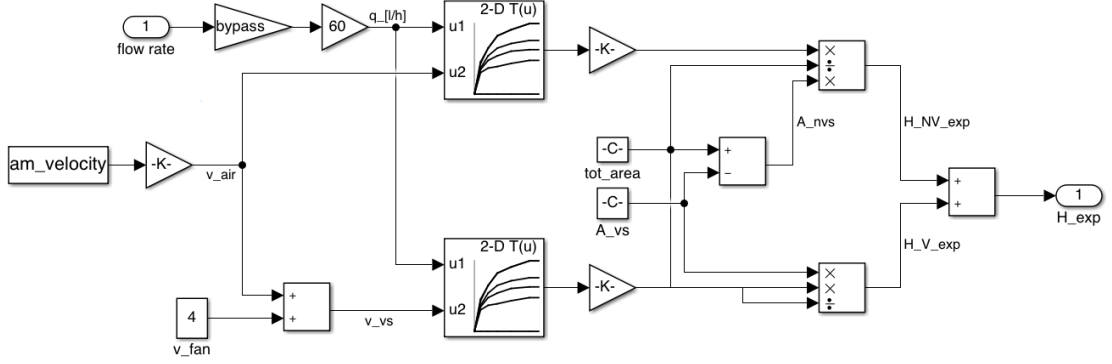


**Figure 3.20:** Experimental heat exchanged subsystem

Once obtained the real heat it is finally possible to calculate the temperature of the coolant leaving the radiator by using again first principle of thermodynamics:

$$T_{out_{radiator}} = T_{out_{coolant}} + \frac{H_{real}}{c_p \cdot dm} \quad (3.34)$$

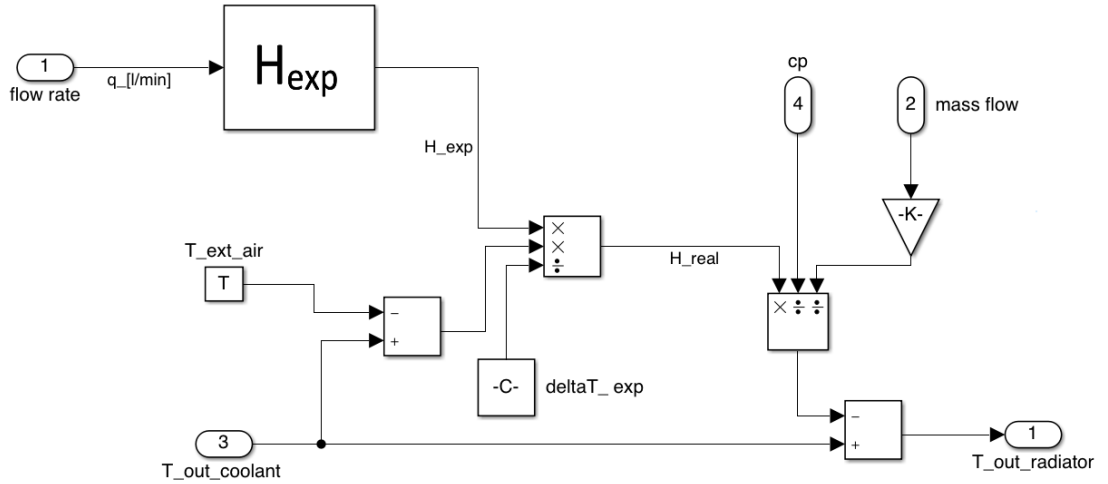


**Figure 3.21:** Radiator subsystem

### 3.2.6 Cooling system control

The optimum range of temperature in which a fuel cell should work is between  $60 - 80\text{ }^{\circ}\text{C}$ . For this reason a strategy control of cooling system is necessary. There are three ways in this model to control the stack temperature:

- regulate centrifugal pump rotation speed, as already discussed in paragraph 3.2.4;
- switch on and off the radiator with a by-pass valve;
- regulate the mass flow rate passing through the radiator.

The radiator turns on when the stack reaches  $60\text{ }^{\circ}\text{C}$  and turns off if  $55\text{ }^{\circ}\text{C}$  are reached. To do so a stateflow block is used. It receives as input  $T_{stack}$ : if  $T_{stack} < 60\text{ }^{\circ}\text{C}$  the output "signal" is 0; when  $T_{stack} > 60\text{ }^{\circ}\text{C}$  it changes state and *signal* becomes 1; it turn back to 0 only when  $T_{stack} < 55\text{ }^{\circ}\text{C}$  is reached.

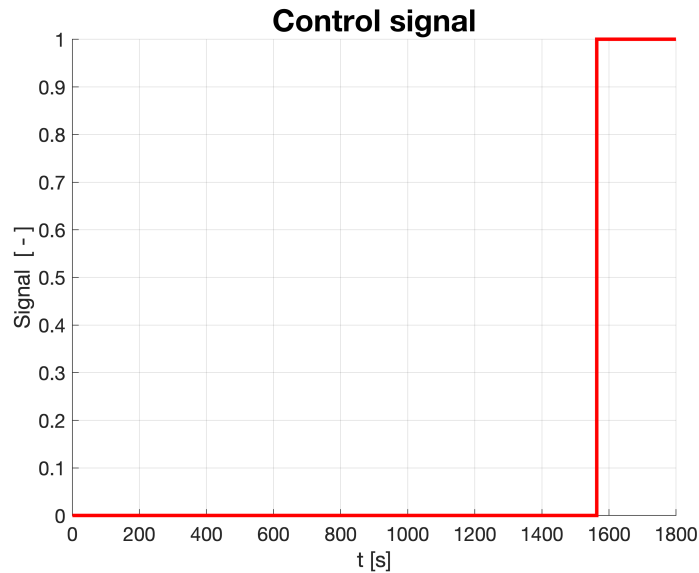


**Figure 3.22:** Output signal generated by control block

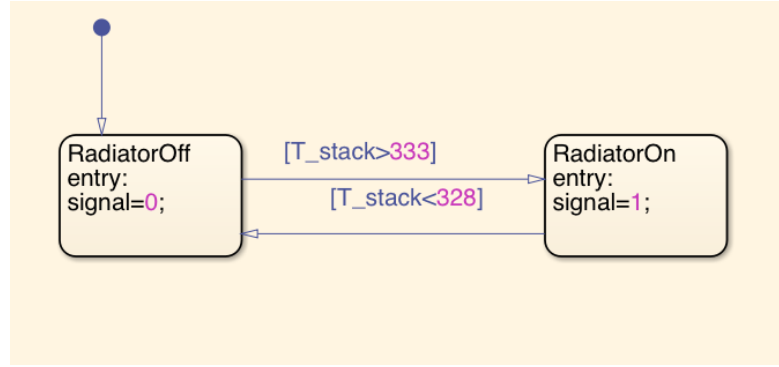


**Figure 3.23:** Radiator control block

After this, a switch block is used: it pass through  $T_{out_{radiator}}$  when signal from control block is higher than 0, otherwise it pass through  $T_{out_{coolant}}$ . In this way the radiator is cutted off from the circuit.

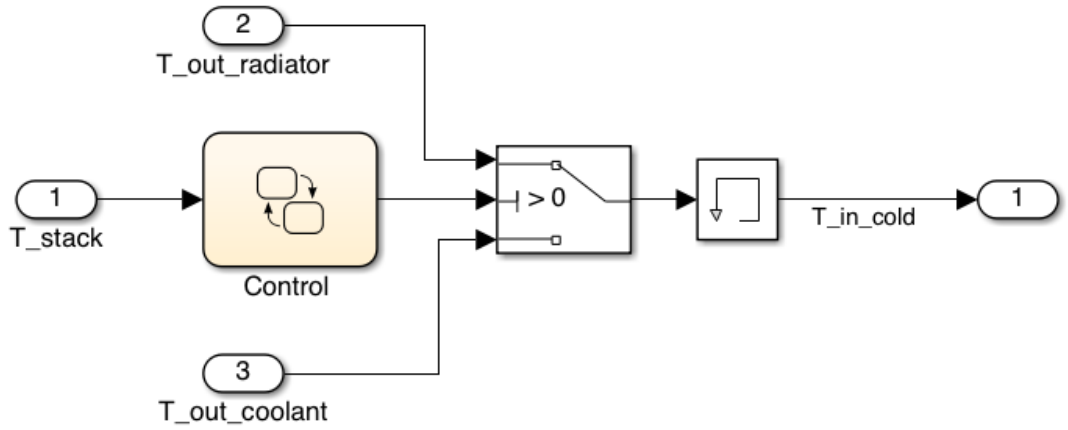


**Figure 3.24:** Radiator control subsystem

To simulate a by-pass valve, the mass flow rate value entering the radiator block is multiplied by a value "*bypass*" that represent the percentage of mass flow rate by-passed. For this reason, once the control block has chosen the correct temperature  $T_{in_{cold}}$ , a weighted mean of the effective temperature of the coolant must be done.

$$T_{in_{coolant}} = T_{out_{coolant}} \cdot (1 - bypass) + T_{in_{cold}} \cdot bypass \quad (3.35)$$



Finally, the mean value  $T_{cool}$  between  $T_{out_{coolant}}$  and  $T_{in_{coolant}}$  is computed in order to calculate the fluid properties of the coolant. In this way the loop is closed

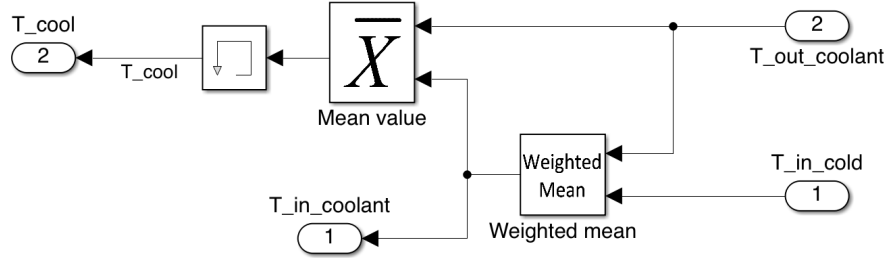


**Figure 3.25:** Coolant inflow subsystem

### 3.3 Model configuration

During the development of the model two algebraic loops emerged.

The first one regards the pump and pressure drops. It has been easily solved by initiating the pressure drop entering the pump with a memory block (see figure 3.16).

The second loop regards the inflow and outflow temperature of coolant. Simulink tries to solve it by assuming the first value of the circuit, but this process brings to instabilities. To overcome this issue the time integration solver of the model is set to *ode4* (Runge-Kutta) with fixed time-step of 0.1.

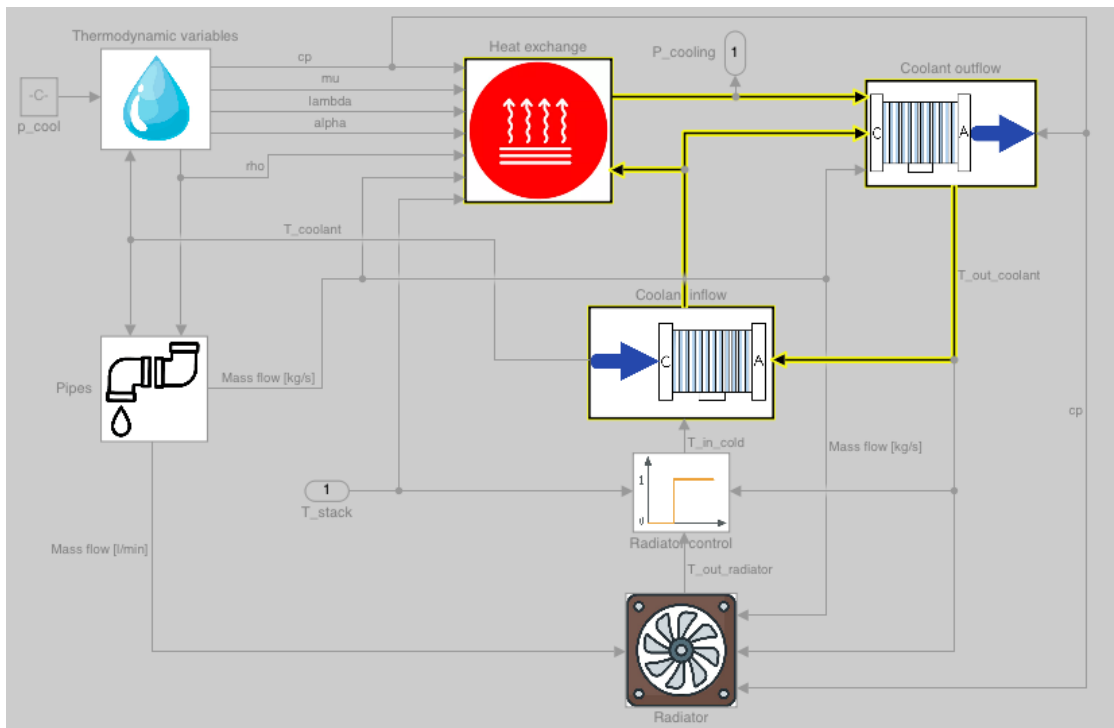


**Figure 3.26:** Overview of the loop

## Chapter 4

# Results

The model is validated with a comparison with Amesim results. Some adjustments are necessary in order to make the two models work with the same set up options and initial conditions. These adjustments are:  
in Amesim model:

- initial temperature set to 20 °C;
- polarization curves provided from Simulink ;
- "generic geometry with user-defined correlations" mode is set for the heat exchange between stack and coolant: by setting this parameter Amesim computes  $h_{conv}$  using equations showed in section 3.2.3;
- heat exchange with reactants is deactivated: because hydrogen and oxygen are compressed before entering anode and cathode respectively, they have higher temperature than the stack. For this reason, the heat exchanged between reactants and stack is not negligible. In Simulink this part hasn't been modelled, thus it is necessary to deactivate it in Amesim in order to have a fair comparison.

in Simulink model:

- initial temperature set to 20 °C;
- coolant absolute pressure set to 1.1 bar;
- centrifugal pump rotating speed set to 200 rpm;
- *bypass* value, entering the radiator, set to 0.4.

In the next few pages the results will be discussed. A bottom to top approach is used by presenting first of all the parameters that involves the heat generation and heat transfer. In the final section the most important result will be showed, which is the stack temperature. The load imposed is a current density load derived by driving the vehicle along a WLTP driving cycle.

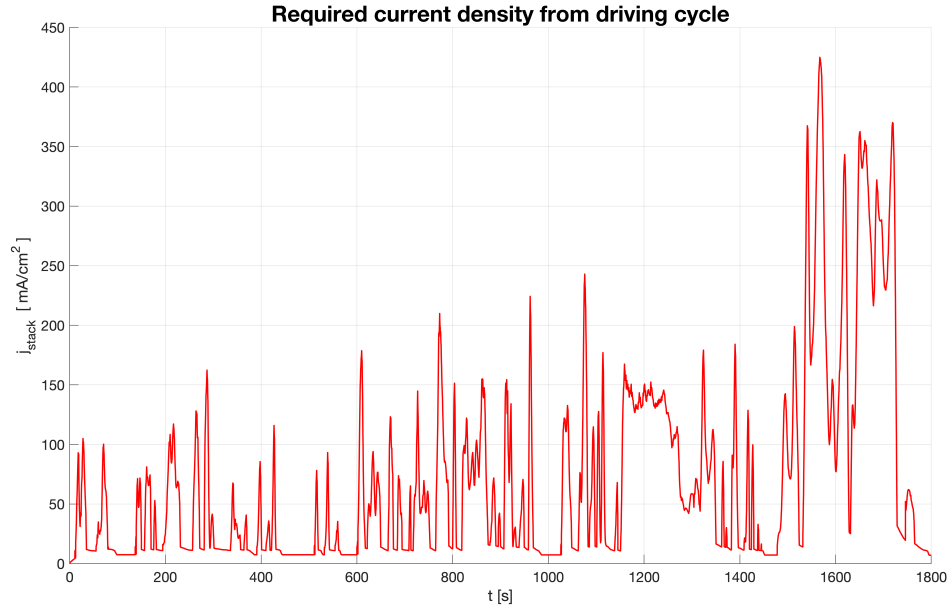


**Figure 4.1:** Current density from WLTP cycle

## 4.1 Heat generation

The calculation of chemical voltage involves the temperature in particular the reactants temperature. By deactivating heat exchange between reactants and stack, the chemical voltage is affected. For this reason, only for plotting figure 4.2 the reactants in Amesim are activated because otherwise the two models wouldn't be comparable.

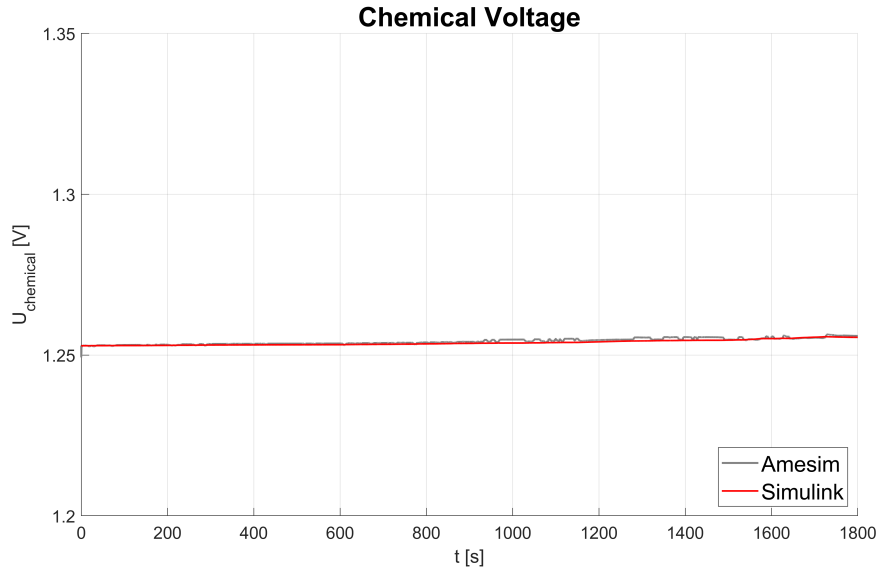


**Figure 4.2:** Chemical voltage

The cell voltage, given by polarization curves, follows the same trend of the reference model as shown in figure 4.3.

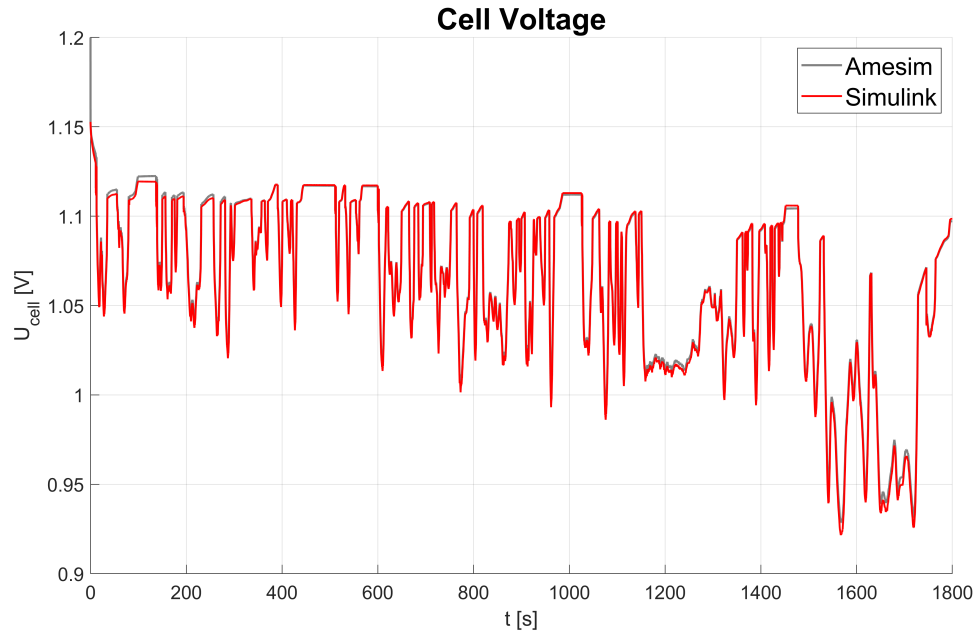


**Figure 4.3:** Cell voltage

Consequently given the chemical voltage and cell voltage, the heat loss computed in section 3.1 is also in good agreement.

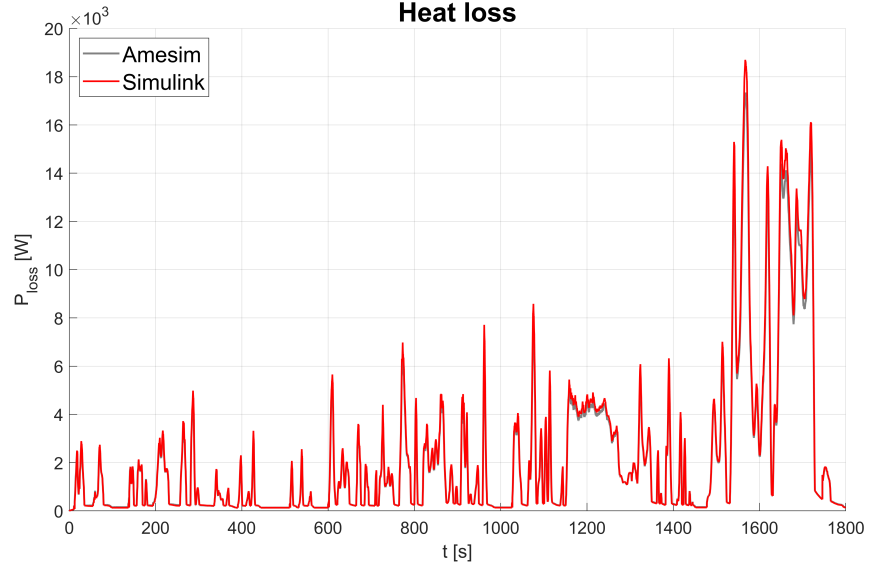


**Figure 4.4:** Heat loss

## 4.2 Heat exchange

The convective heat exchange coefficient is shown in figure 4.5. Although it has the same trend and order of magnitude, there is a constant relative error of about 15 %.

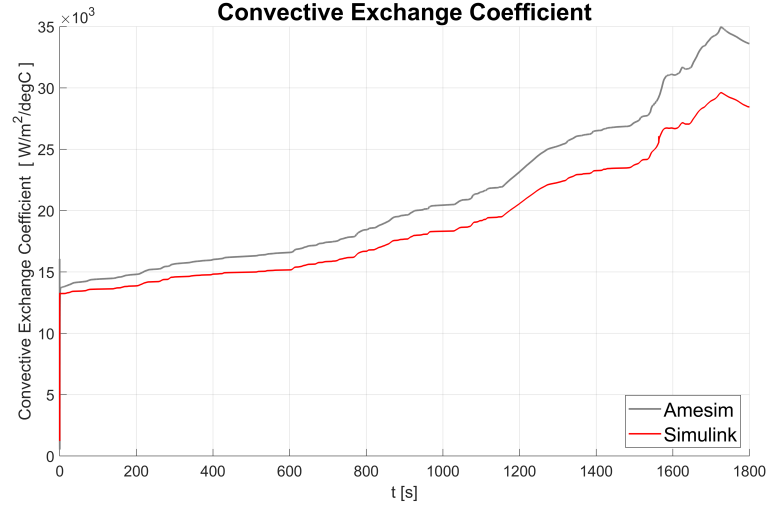


**Figure 4.5:** Convective heat exchange coefficient

This error derives from the same relative error on the Nusselt number, as it will be discussed later on.

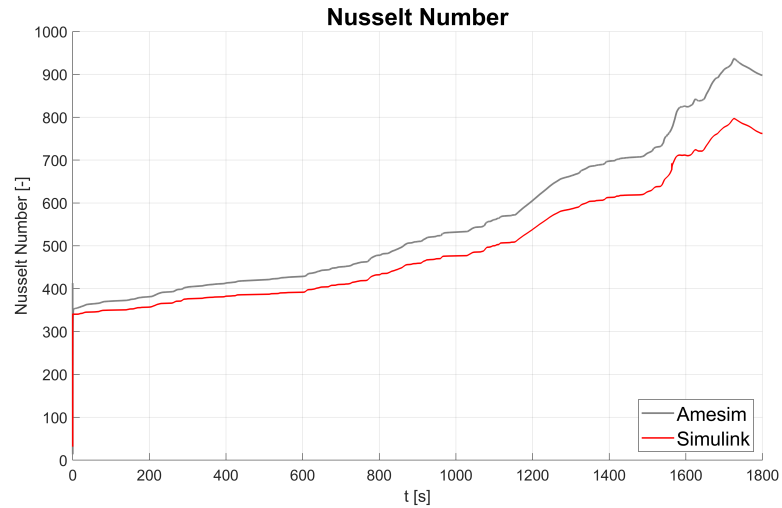


**Figure 4.6:** Nusselt number

The Nusselt number depends on Reynolds, Prandtl, Grashof and the friction factor, reported respectively in figures 4.7, 4.8, 4.9 and 4.10.

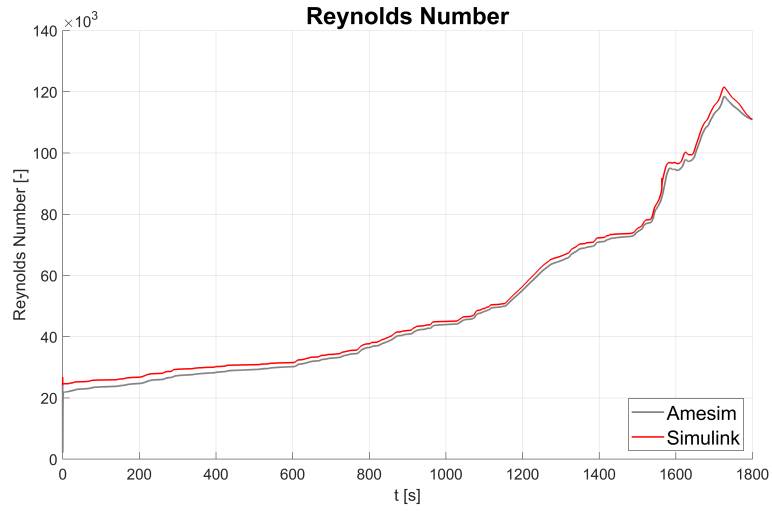


Figure 4.7: Reynolds number

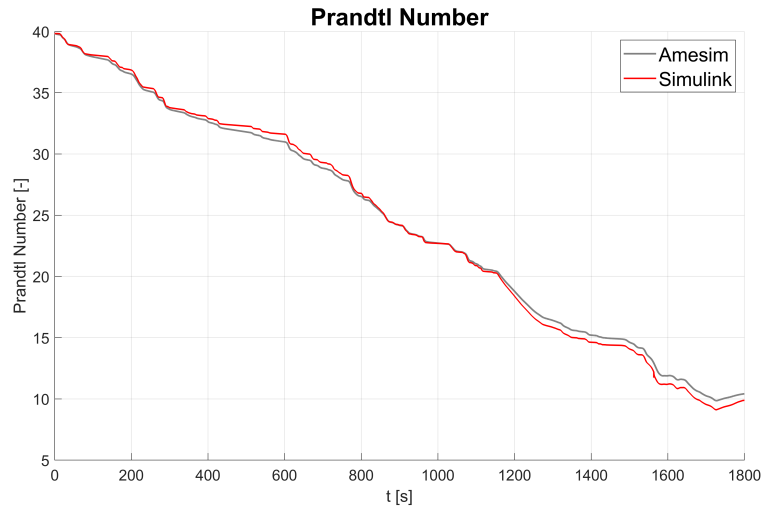
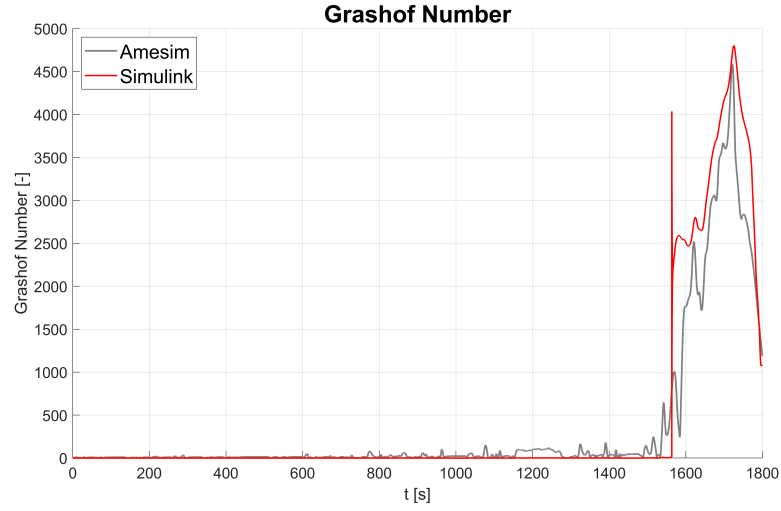
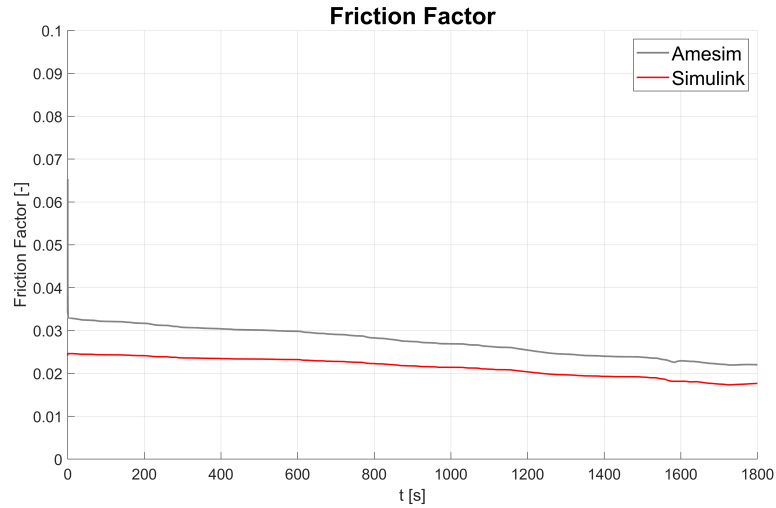


Figure 4.8: Prandtl number



**Figure 4.9:** Grashof number**Figure 4.10:** Friction factor

From this analysis the friction factor is the parameter that presents a deviation between the two models. In fact the data that the reference model use to calculate the friction factor were not available and a different source of the Moody Diagram was chosen. To further investigate and confirm this hypothesis a simple test was done. The friction factor from the reference model was imposed and the Nusselt number presented the same values, the result of this test are shown in Appendix.

### 4.3 Pump and pressure drops

The pressure drops in Amesim model are a order of magnitude higher than the literature values. For this reason, after multiple attempts of matching the pressure drops it has been decided to use a table to calculate them. This choice was done in order to have the mass flow rate similar in both models because it affects the overall system. To do this, the centrifugal pump is regulated to reach the goal.

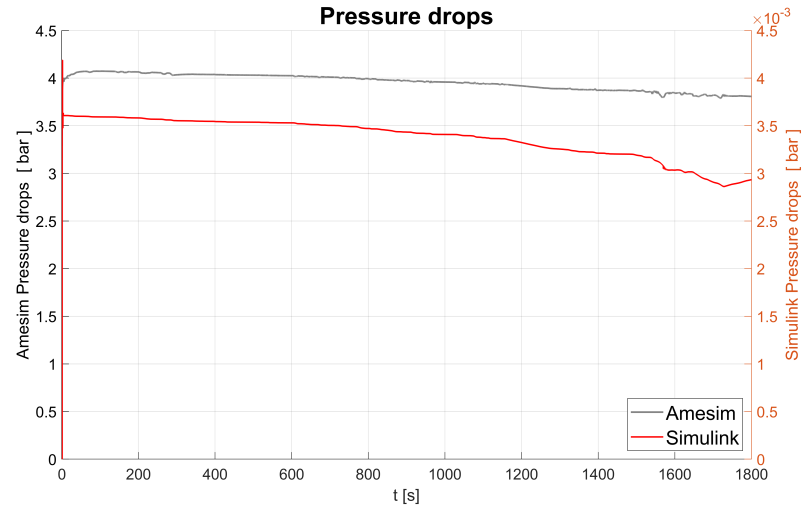


Figure 4.11: Pressure drops comparison

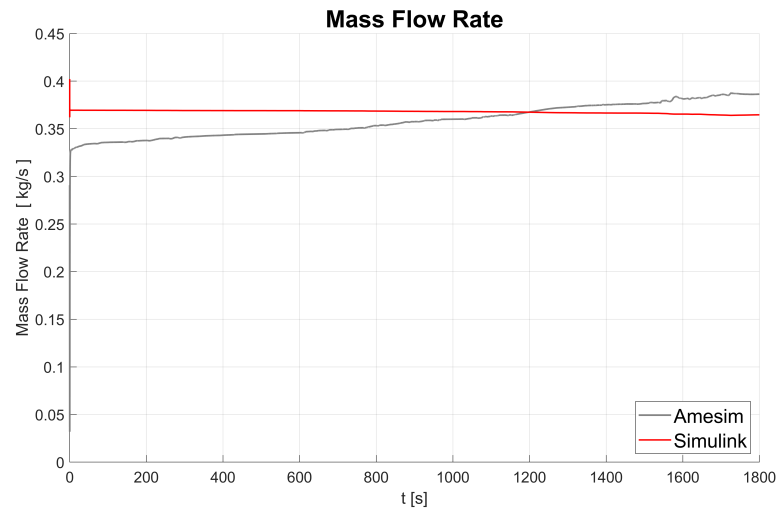
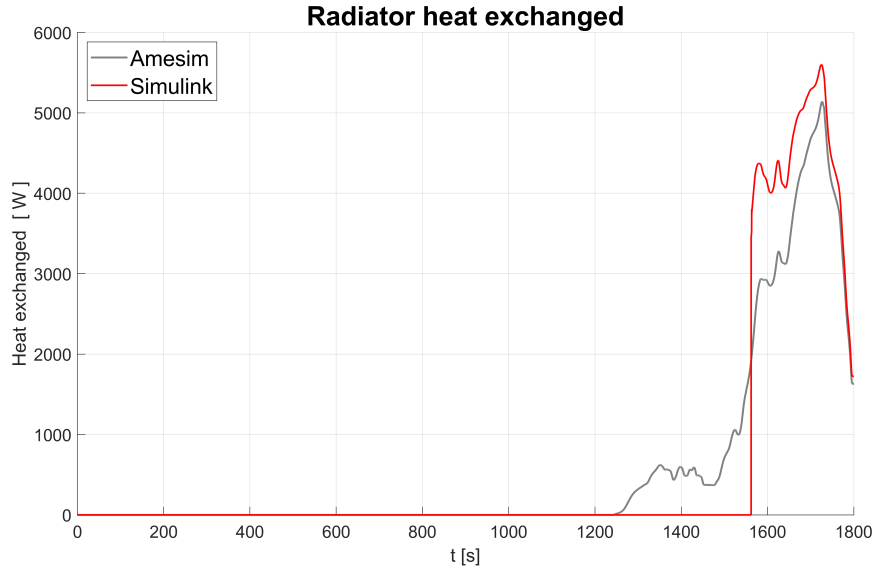


Figure 4.12: Mass flow rate

## 4.4 Radiator

The value of the temperature remains under the thresholds of 60 degree Celsius until about 1600 seconds. From this value on, coolant will pass through the radiator where will be cooled down. While in Simulink the mass flow rate by-passed is constant in Amesim it is controlled by a thermostatic valve. For this reason, the mass flow rate is gradually increasing and with it so does also the heat exchange. As can be observed in figure 4.13, the heat exchange is starting after 1200 s but there is no influence on the temperature. At 1600 s the thermostatic valve completely opens and the values from the two models become comparable. The differences between the two models can be thus attributed to the control strategies.



**Figure 4.13:** Radiator heat exchange

## 4.5 Temperature

Finally the temperature trend is analyzed. This is the most important variable to consider because it affects the performance of the fuel cell. As shown in figure 4.14 the two curves are both in good agreement. The difference, whose maximum error is 3%, can be attributed to the properties of the fluid. In fact, these values cannot be compared because in Amesim are not available. However, the error is acceptable within the aim of the dissertation.

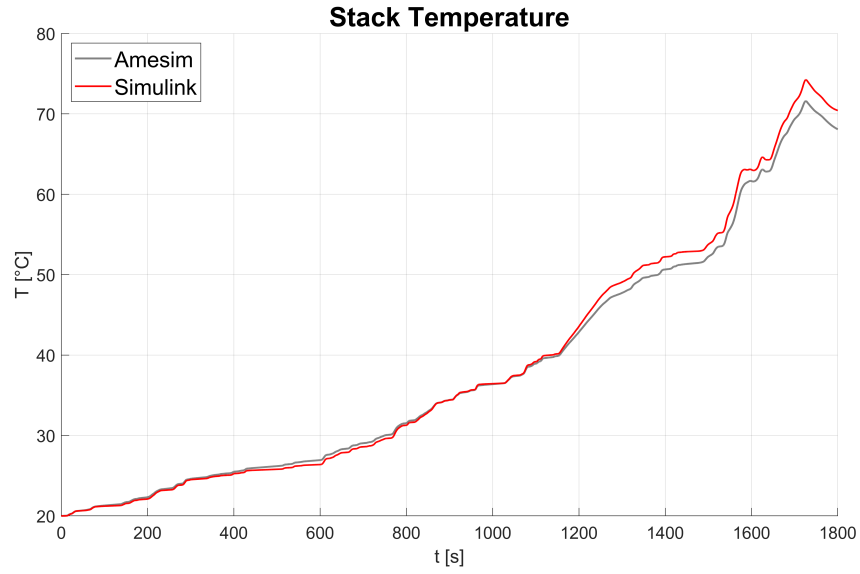


**Figure 4.14:** Stack temperature

Figure 4.15 shows the radiator starting time: it switches on after about 1550 s when the stack reaches 60 °C.

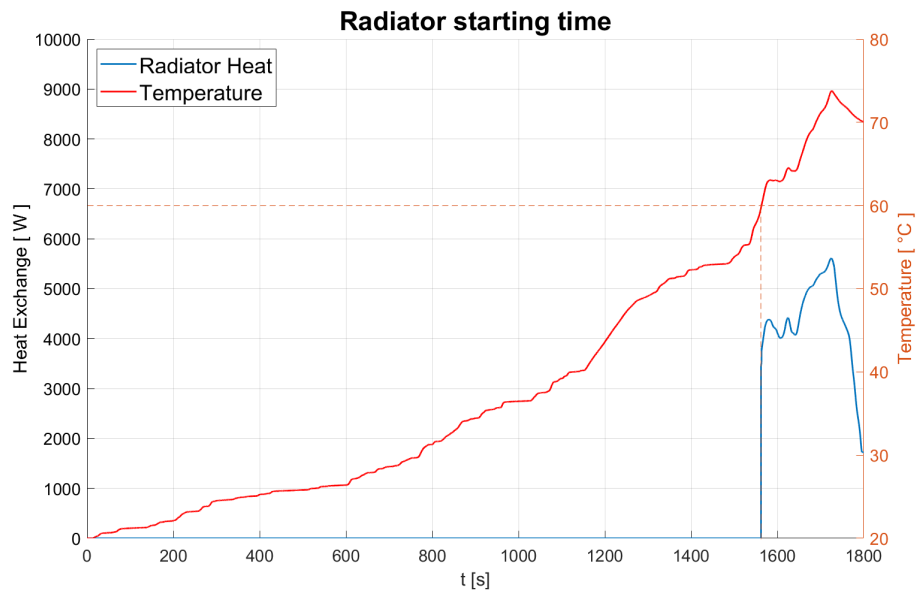


**Figure 4.15:** Focus on radiator starting time

To highlight the importance of the radiator, figure 4.16 is plotted. It shows

the temperature with the radiator switched on and off. Without this device it is evident that temperature exceeds the threshold of  $80\text{ }^{\circ}\text{C}$  and the fuel cell could be damaged.

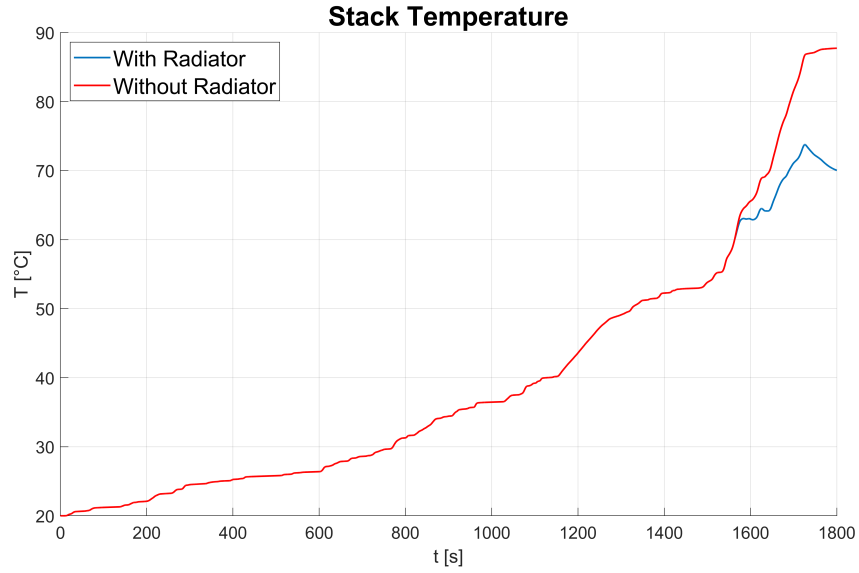


**Figure 4.16:** Example of how the radiator affects the temperature

## Chapter 5

# Conclusions

The thesis activity aimed at develop and validate a thermal model of a fuel cell system for an electric vehicle in Simulink. The work was divided into two parts.

The first part was focused on modelling the FC heat generation by calculating theoretical voltage, subtracting voltage from polarization curves and finally multiplying this difference by the current.

The second part aimed at modelling the cooling system. Fluid thermodynamic properties were computed, as well as the convective heat exchange between stack and coolant. A centrifugal pump and a radiator were then integrated. Finally, a system control was implemented in order to maintain the fuel cell between 60 and 80 °C.

To validate the model, a Siemens software has been used, namely Simcenter Amesim.

Regarding the heat generation, the model, based on the calculation of the chemical voltage and the cell voltage, has shown good agreement with the reference. Consequently, the heat loss was coherent and numerical values had very low error.

The cooling system presented more issues, given by the absence of some variables in Amesim, for instance the fluid properties. Although adimensional numbers showed good reliability, Nusselt number and convective heat exchange coefficient exhibited a consistent discrepancy with the reference. This error is led by the different type of computation of the friction factor. While the radiator gave suitable results, the pressure drops were three order magnitude lower than Amesim. This error was allowed because those values permitted to better calibrate the mass flow rate. In fact, mass flow rate was a more important value and it was in good agreement with the reference. To conclude, the model gave good results in terms of temperature calculation. The maximum error was 3% and could be attributed to the fluid properties that were the only parameters that couldn't be compared with Amesim.

Other future work on the topic could be focused on:

- integrate the reactants feeding system in order to calculate the heat exchange between them and the stack;
- adapt the entire model to a heavy-duty vehicle: two stacks in series are required and centrifugal pump and radiator must be resized;
- once re-adapted the model, integrate it into a hybrid powertrain of a heavy-duty vehicle and study optimal control strategy.

## Appendix A

# Convective heat exchange coefficient

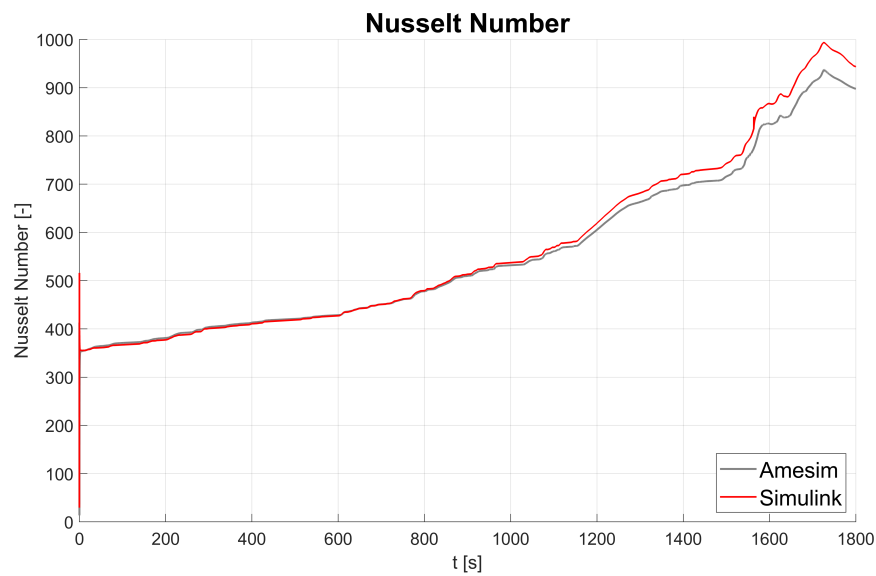


**Figure A.1:** Nusselt number with friction factor and mass flow rate from Amesim



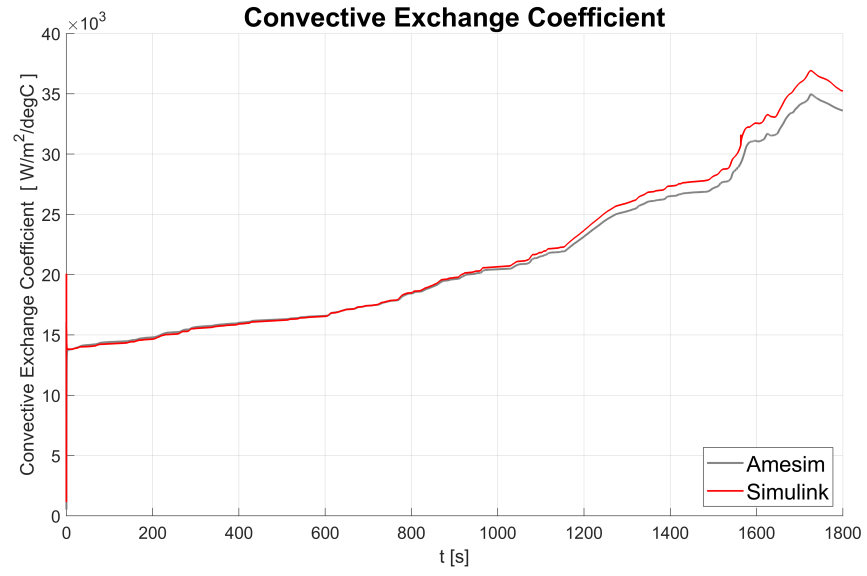


**Figure A.2:** Convective heat exchange coefficient with friction factor and mass flow rate from Amesim

# Bibliography

- [1] Ahluwalia R.K. et al. Cullen D.A. Neyerlin K.C. «New roads and challenges for fuel cells in heavy-duty transportation». In: (). Ed. by 462–474 (2021) *Nat Energy* 6. DOI: <https://doi.org/10.1038/s41560-021-00775-z> (cit. on p. 2).
- [2] Frano Barbir. *PEM Fuel Cells, Theory and Practice*. Ed. by Frano Barbir. Burlington: Academic Press, 2005. ISBN: 978-0-12-078142-3. DOI: <https://doi.org/10.1016/B978-0-12-078142-3.X5000-9>. URL: <https://www.sciencedirect.com/book/9780120781423/pem-fuel-cells> (cit. on pp. 4, 7, 9, 11–15, 17–19).
- [3] A. Miraoui F. Gao B. Blumier. *Proton Exchange Membrane Fuel Cells Modeling*. Ed. by Willey (cit. on pp. 4, 7).
- [4] A. Sciarretta L. Guzzella. *Vehicle Propulsion Systems*. Ed. by Springer (cit. on p. 4).
- [5] Andrei A. Kulikovsky. «Chapter 1 - Fuel cell basics». In: *Analytical Modeling of Fuel Cells (Second Edition)*. Ed. by Andrei A. Kulikovsky. Second Edition. Elsevier, 2019, pp. 1–33. ISBN: 978-0-444-64222-6. DOI: <https://doi.org/10.1016/B978-0-44-64222-6.00008-3>. URL: <https://www.sciencedirect.com/science/article/pii/B9780444642226000083> (cit. on p. 5).
- [6] *Cost-efficient production of bipolar plates for fuel cells*. URL: <https://phi-hannover.de/en/cost-efficient-production-of-bipolar-plates-for-fuel-cells/> (cit. on p. 6).
- [7] *A One-Dimensional Heat, Mass and Charge Transfer Model for a Polymer Electrolyte Fuel Cell Stack*. URL: <https://www.fuelcellstore.com/blog-section/heat-mass-charge-transfer-model-pem-fuel-cell> (cit. on p. 8).
- [8] Mohamed H.S. Bargal, Mohamed A.A. Abdelkareem, Qi Tao, Jing Li, Jianpeng Shi, and Yiping Wang. «Liquid cooling techniques in proton exchange membrane fuel cell stacks: A detailed survey». In: *Alexandria Engineering Journal* 59.2 (2020), pp. 635–655. ISSN: 1110-0168. DOI: <https://doi.org/>

- 10.1016/j.aej.2020.02.005. URL: <https://www.sciencedirect.com/science/article/pii/S1110016820300600> (cit. on pp. 19, 20).
- [9] Siemens Amesim. «Fuel Cell System Integration in a FCEV». In: (). Ed. by Fuel Cell library (cit. on p. 21).
- [10] Michael J. Zehe Bonnie J. McBride and Sanford Gordon. «NASA Glenn Coefficients for Calculating Thermodynamic Properties of Individual Species». In: (). Ed. by NASA (cit. on p. 23).
- [11] SAE International, ed. *Aerospace Hydraulic Fluids Physical Properties AIR1362B* (cit. on p. 27).
- [12] *Thermophysical Properties of Fluid Systems*. URL: <https://webbook.nist.gov/chemistry/fluid/> (cit. on p. 28).
- [13] Incropera F. Bergman T.L. DeWitt D.P. and Lavine A.S. *Fundamentals of Heat and Mass Transfer*. Vol. 997. Jan. 2011. ISBN: 9780470501979 (cit. on p. 32).



# Acknowledgements

A conclusione di questo elaborato, desidero menzionare tutte le persone senza le quali questo lavoro di tesi non esisterebbe.

Innanzitutto ringrazio i miei relatori Daniela Misul e Giovanni Belingardi per la fiducia riposta in me e per i preziosi consigli datimi.

Un ringraziamento particolare va ai correlatori Pier Anselma e Matteo Spano. Grazie per aver condiviso le vostre conoscenze, avermi guidata nel lavoro di tesi e soprattutto grazie per la pazienza.

Infine ringrazio il mio collega Marco Capello per aver condiviso con me questo percorso e per il reciproco sostegno.